AD-A174 338 CERENKOV RADIATION TRANSITION RADIATION AND DIFFRACTION 1/1
TRANSITION RADIAT..(U) NAVAL POSTGRADUATE SCHOOL
MONTEREY CA A J O'GRADY JUN 86

UNCLASSIFIED F/G 20/6 NL

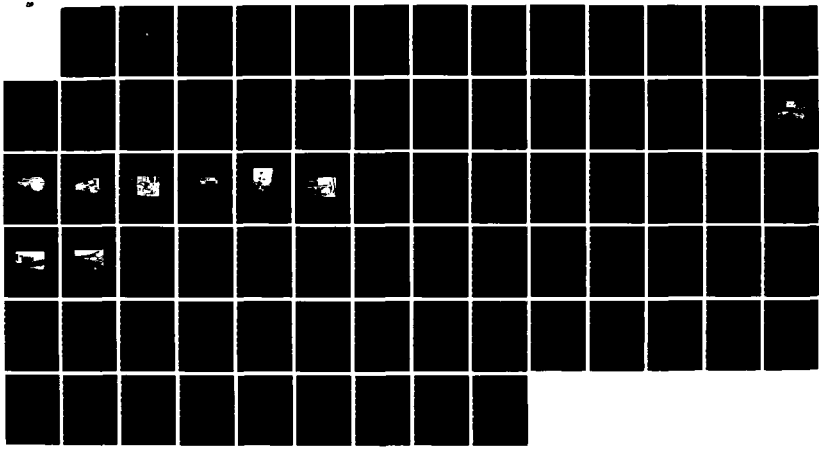

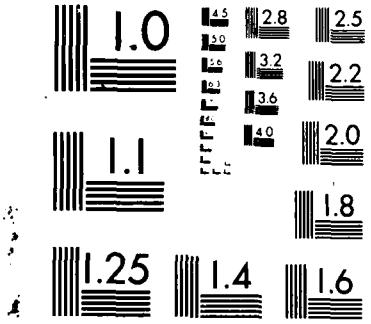

(2)

NAVAL POSTGRADUATE SCHOOL

Monterey, California

THESIS

CERENKOV RADIATION, TRANSITION RADIATION AND DIFFRACTION TRANSITION RADIATION FROM PERIODIC BUNCHES FOR A FINITE BEAM PATH IN AIR

by

Arthur J. O'Grady

June 1986

Thesis Advisor: Fred R. Buskirk

Approved for public release; distribution is unlimited

UNCLASSIFIED

SECURITY CLASSIFICATION OF THIS PAGE

REPORT DOCUMENTATION PAGE

1a REPORT SECURITY CLASSIFICATION UNCLASSIFIED	1b RESTRICTIVE MARKINGS #174338
2a SECURITY CLASSIFICATION AUTHORITY	3 DISTRIBUTION / AVAILABILITY OF REPORT Approved for public release; distribution is unlimited
2b DECLASSIFICATION / DOWNGRADING SCHEDULE	
4 PERFORMING ORGANIZATION REPORT NUMBER(S)	5 MONITORING ORGANIZATION REPORT NUMBER(S)
6a NAME OF PERFORMING ORGANIZATION NAVAL POSTGRADUATE SCHOOL	6b OFFICE SYMBOL (If applicable) Code 61
7a NAME OF MONITORING ORGANIZATION Naval Postgraduate School	
6c ADDRESS (City, State, and ZIP Code) Monterey, California 93943-5000	7b ADDRESS (City, State, and ZIP Code) Monterey, California 93943-5000
8a NAME OF FUNDING / SPONSORING ORGANIZATION	8b OFFICE SYMBOL (If applicable)
9 PROCUREMENT INSTRUMENT IDENTIFICATION NUMBER	
8c ADDRESS (City, State, and ZIP Code)	10 SOURCE OF FUNDING NUMBERS PROGRAM ELEMENT NO / PROJECT NO / TASK NO / WORK UNIT ACCESSION NO

11 TITLE (Include Security Classification)
CERENKOV RADIATION, TRANSITION RADIATION AND DIFFRACTION TRANSITION RADIATION FROM PERIODIC BUNCHES FOR A FINITE BEAM PATH IN AIR

12 PERSONAL AUTHOR(S)
O'Grady, Arthur J.

13a TYPE OF REPORT	13b TIME COVERED	14 DATE OF REPORT (Year, Month, Day)	15 PAGE COUNT
Master's Thesis	FROM _____ TO _____	1986, June	76

16 SUPPLEMENTARY NOTATION

17 COSATI CODES			18 SUBJECT TERMS (Continue on reverse if necessary and identify by block number)
FIELD	GROUP	SUB-GROUP	Cerenkov Radiation; Transition Radiation; Diffraction Transition Radiation

19 ABSTRACT (Continue on reverse if necessary and identify by block number)

Cerenkov, transition and diffraction transition radiation generated diffraction patterns are analyzed in order to determine whether a functional angular dependence exists to differentiate between these radiations. Experimental evidence is presented demonstrating differences in the diffraction pattern after specific changes are made during the experiment to identify transition radiation and diffraction transition radiation effects. Upon comparison with theoretical plots of Cerenkov radiation patterns, all three radiation effects can be isolated. This is significant in that there are no absolute boundaries between these three radiations and furthermore, Cerenkov radiation merges into transition radiation for a finite path length. Additionally, improvements in noise reduction in data recording have been made which lend further support to the validity of the equation for the power in the diffraction pattern of Cerenkov radiation from periodic

20 DISTRIBUTION / AVAILABILITY OF ABSTRACT	21 ABSTRACT SECURITY CLASSIFICATION
☒ UNCLASSIFIED/UNLIMITED ☐ SAME AS RPT ☐ DTIC USERS	Unclassified
22a NAME OF RESPONSIBLE INDIVIDUAL Prof. Fred R. Buskirk	22b TELEPHONE (Include Area Code) (408 646-2765
22c OFFICE SYMBOL Code 61Bs	

DD FORM 1473, 84 MAR 83 APR edition may be used until exhausted
All other editions are obsolete

SECURITY CLASSIFICATION OF THIS PAGE
UNCLASSIFIED

#19 - ABSTRACT - (CONTINUED)

bunches for a finite path in air as derived by Neighbours and Buskirk. It is also proposed that postulated noise-generated fine structure in previous experiments at NPSAL is partly caused by inherent transition and diffraction transition radiation.

Approv for public release; distribution is unlimited.

Cerenkov Radiation, Transition Radiation and Diffraction Transition Radiation from Periodic Bunches for a Finite Beam Path in Ai

by

Arthur J. O'Grady
Lieutenant Commander, United States Navy
B.A. University of Rochester, 1972

Submitted in partial fulfillment of the requirements for the degree of

Master of Science in Physics

from the

Naval Postgraduate School
June 1986

Author: _____
Arthur J. O'Grady

Approved by: _____
Fred R. Buskirk, Thesis Advisor

_____
John R. Neighbours, Second Reader

_____
G. E. Schacher, Chairman
Department of Physics

_____
J. N. Dyer
Dean of Science and Engineering

ABSTRACT

Cerenkov, transition and diffraction transition radiation generated diffraction patterns are analyzed in order to determine whether a functional angular dependence exists to differentiate between these radiations. Experimental evidence is presented demonstrating differences in the diffraction pattern after specific changes are made during the experiment to identify transition radiation and diffraction transition radiation effects. Upon comparison with theoretical plots of Cerenkov radiation patterns, all three radiation effects can be isolated. This is significant in that there are no absolute boundaries between these three radiations and furthermore, Cerenkov radiation merges into transition radiation for a finite path length. Additionally, improvements in noise reduction in data recording have been made which lend further support to the validity of the equation for the power in the diffraction pattern of Cerenkov radiation from periodic bunches for a finite path in air as derived by Neighbours and Buskirk. It is also proposed that postulated noise-generated fine structure in previous experiments at NPSAL is partly caused by inherent transition and diffraction transition radiation.

TABLE OF CONTENTS

A-1

I. INTRODUCTION

A. BACKGROUND

1. History

The term Cerenkov radiation was first used in 1940, although its effects were observed by Mme. Curie in 1910. While performing her research with radioactivity, Mme. Curie noted that bottles of concentrated radium solutions were emitting a bluish-white or pale blue light. It was not until 1937 that Frank and Tamm theorized the origin of Cerenkov radiation which takes its name from Pavel A. Cerenkov, who performed a complete set of experiments dealing with this phenomenon from 1934 to 1938. The results of his experiments were in excellent agreement with the theory of Frank and Tamm. In the interim, Mallet was the first individual to begin actively studying this phenomenon between the years 1926 and 1929, although it appears Cerenkov was unaware of Mallet's earlier work. Both individuals stumbled upon this phenomenon accidently while studying fluorescence and other forms of luminescence. Ginzburg in 1940 made the next contribution to understanding this phenomenon when he produced its quantum theory. Following this, it became known as Cerenkov radiation. In 1958, J.V. Jelley wrote a complete work on Cerenkov radiation covering theory through current

research [Ref. 1]. Cerenkov radiation owes its importance to its ability to detect a charged particle and measure its speed.

In the original theory put forth by Frank and Tamm [Ref. 1], they assumed infinite media and constant velocity. In actuality both the medium traversed and the length of the particle's path are finite. The finite path introduces diffraction effects and the boundaries of the medium changes the total radiation yield, adding a small contribution to the Cerenkov radiation known as Transition Radiation.

Another form of radiation can be introduced considering charged particles entering a hole in a screen or approaching near a screen. The radiation produced is known as Diffraction Transition Radiation or Diffraction Radiation [Ref. 2]. This was discovered much more recently and is associated with transition radiation. The theory describing diffraction radiation caused by a beam of bunched charged particles is still quite tentative, with little experimental verification.

It appears that the only method available to distinguish between Cerenkov, transition and diffraction transition radiation will be through an analysis of changes generated in the angular dependence of the diffraction pattern.

2. Brief Theory of Cerenkov Radiation

Cerenkov radiation results when a charged particle moves through a dielectric medium (e.g., air, water, glass,

etc.) faster than the phase velocity of light through the same medium. The charged particle causes the medium along its track to be momentarily polarized and generates a short electromagnetic pulse to each elemental region of the medium along the track. The fields then propagate to large distances, as radiation, but only if v is greater than c' [Ref. 1]. The radiation propagates at the Cerenkov angle, $\cos \theta_c = \frac{c'}{v}$, where $c' = c/n$, n is the refractive index of the medium and c is the speed of light in vacuo.

The charged particle in Cerenkov radiation calculations is assumed to pass through a medium of infinite extent, with the observation of radiation occurring at infinity. To determine the radiated power, the electric and magnetic fields must be derived using the scalar and vector potential forms of the associated wave equations which are produced by the charge density and current of the particle. A detailed account is provided by Jelley [Ref. 1]. This analysis culminates with the basic equation for an infinite radiation output (Equation (2.17), [Ref. 1]) because no frequency cutoff was imposed in its derivation and an infinite spectra, representing energy radiated through a cylinder of length ℓ, where the cylinder axis and path of electron are coincident (in cgs units).

$$\frac{dW}{d\ell} = \frac{e^2}{c^2} \int_{\beta n > 1} (1 - \frac{1}{\beta^2 n^2}) \omega \, d\omega$$

In small regions of the spectrum, real media can be assumed dispersionless, although, in reality all media are dispersive. Thus absorption bands exist, and the frequency range in the above equation is then limited to a region below the absorption bands, which then makes the radiated energy finite.

Coherence of the radiation occurs only at the angle θ_c. The radiation field moves a shorter distance ($c'\Delta t$) during a time increment of Δt than does the particle ($v\Delta t$). This relative movement has been likened to the wake of a ship or the shock wave generated by an object in air travelling faster than the speed of sound. Jelley uses the Huygen's principle to explain the wave front coherency [Ref. 1].

Since Cerenkov radiation occurs in three dimensions, the wave front takes the shape of a cone (Figure 2.3, [Ref. 1]). It is important to note that the distribution of intensity of Cerenkov radiation varies directly with the frequency, therefore at microwave frequencies the radiation produced would be difficult to detect unless a bunched and intense electron beam is used, such as the electron accelerator of the Naval Postgraduate School Accelerator Laboratory (NPSAL). This type of radio frequency accelerator produces electron bunches spread 10 centimeters apart and about 1 centimer long. The bunches produce coherent Cerenkov radiation for wavelengths longer than the bunch size.

The power of Cerenkov radiation from periodic electron bunches in a medium of finite interaction length was calculated by Buskirk and Neighbours [Ref. 3], in work accomplished at NPSAL in 1982. Expanding their study a year later, Neighbours and Buskirk calculated the diffraction effects in Cerenkov radiation [Ref. 4]. This work resulted in the following relation for the diffracted power per unit solid angle radiated at the frequency ν,

$$W(\nu,\hat{n}) = \frac{\mu}{2c} L^2 \nu^2 \nu_o^2 \sin^2\theta \left|\underset{\sim}{\rho}_o'(\vec{k})\right|^2 I(u) \qquad (1)$$

which simplifies in watts/steradian [Ref. 5] to

$$W(\nu,\hat{n}) = \nu_o^2 Q R^2 \quad \text{(watts/steradian)} \qquad (2)$$

where:

$Q = \frac{\mu c}{8\pi} q^2$

q = charge in electron bunch

ν_o = frequency of the NPSAL Linac (2.86 GHz)

$R = k L \sin\theta\, I(u) F(\vec{k})$

and where:

$k = \frac{2\pi}{\lambda}$, wave number of Cerenkov radiation

$= jk_o$ (k_o = wave number for ν_o), j = integer

L = finite interaction beam length

$$I(u) = \frac{\sin u}{u} = \text{diffraction pattern function}$$

where:

$$u = \frac{kL}{2}(\cos \theta_c - \cos \theta)$$

$F(\vec{k})$ = form factor of the charge distribution bunch.

The significance of Equation (2) is that the radiated power depends upon the angle, θ, measured to the beam in accordance with the diffraction pattern function, I(u). The form factor, $F(\vec{k})$, will be considered unity because the bunch length of the electron beam is small compared to the operative radiation wavelength. The operating characteristics of the NPSAL electron accelerator are contained in Appendix A.

Since the theory is developed for the far field, it is important to perform experiments in this regime. The distance to the far field r, for the microwave region, is determined by the relation [Ref. 6]:

$$r = \frac{2L^2}{\lambda} \tag{3}$$

where λ is the wavelength of the radiation being investigated. For a far field experiment, r must be limited by the confines of the experimental end station of NPSAL as illustrated in Figure 1 and L is the region of interaction between the beam and the medium. The interaction region L and harmonic number can both be varied to give a range of

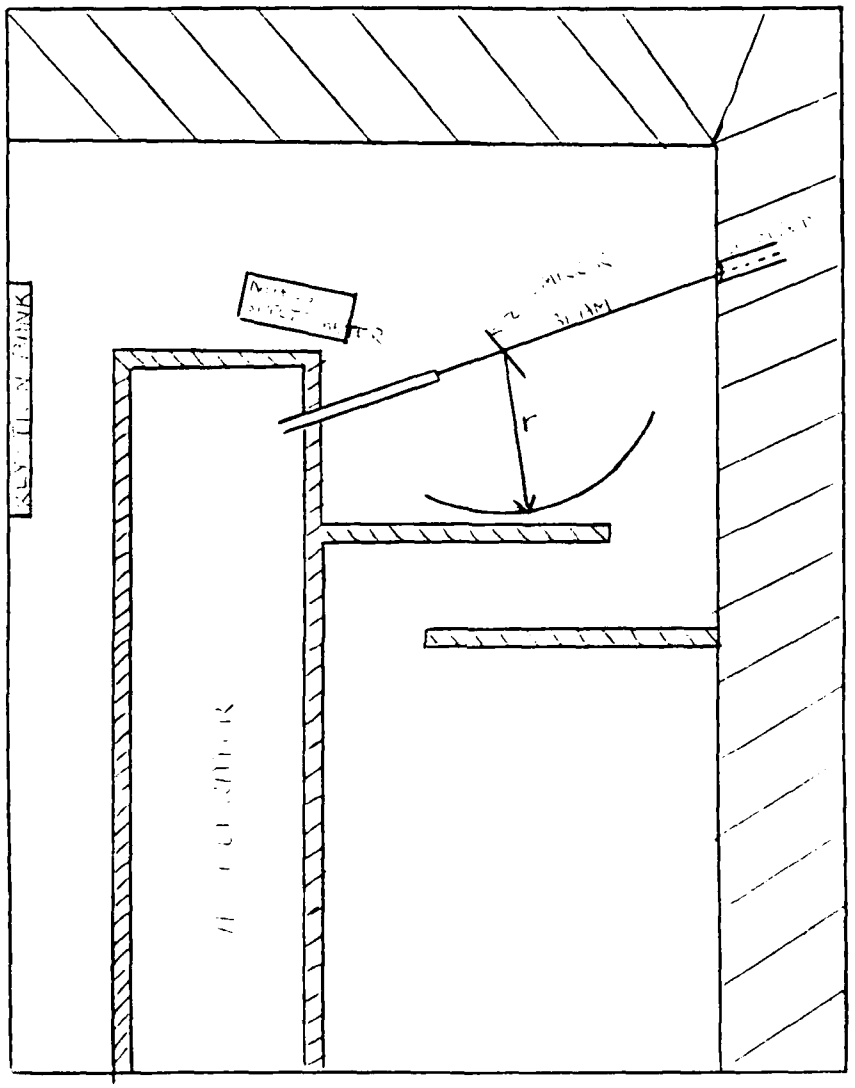

Figure 1. NPSAL Experimental End Station

r. The distance to the far field is calculated using Equation (3) for several interaction lengths for the third harmonic (J = 3) and displayed in Table 1.

TABLE 1

DISTANCE TO THE FAR FIELD FOR J = 3

L (meters)	r (meters)
0.07	0.28
0.14	1.12
0.21	2.52
0.42	10.08
1.00	57.14

Using the parameters from Appendix A and the 0.14 meters result of Table 1, the Cerenkov radiation diffraction pattern determined from Equation (2) is plotted as calculated by Neighbours' CERE 10 computer program. Several previous experiments have been conducted at NPSAL to verify Equation (2) which culminated with Bruce's work [Ref. 5].

The experiment completed by Bruce in 1985 essentially validated Equation (2) through improvements in noise reduction and data collection. However, his results contained aberrations in the diffraction patterns which were attributed to unresolved noise problems.

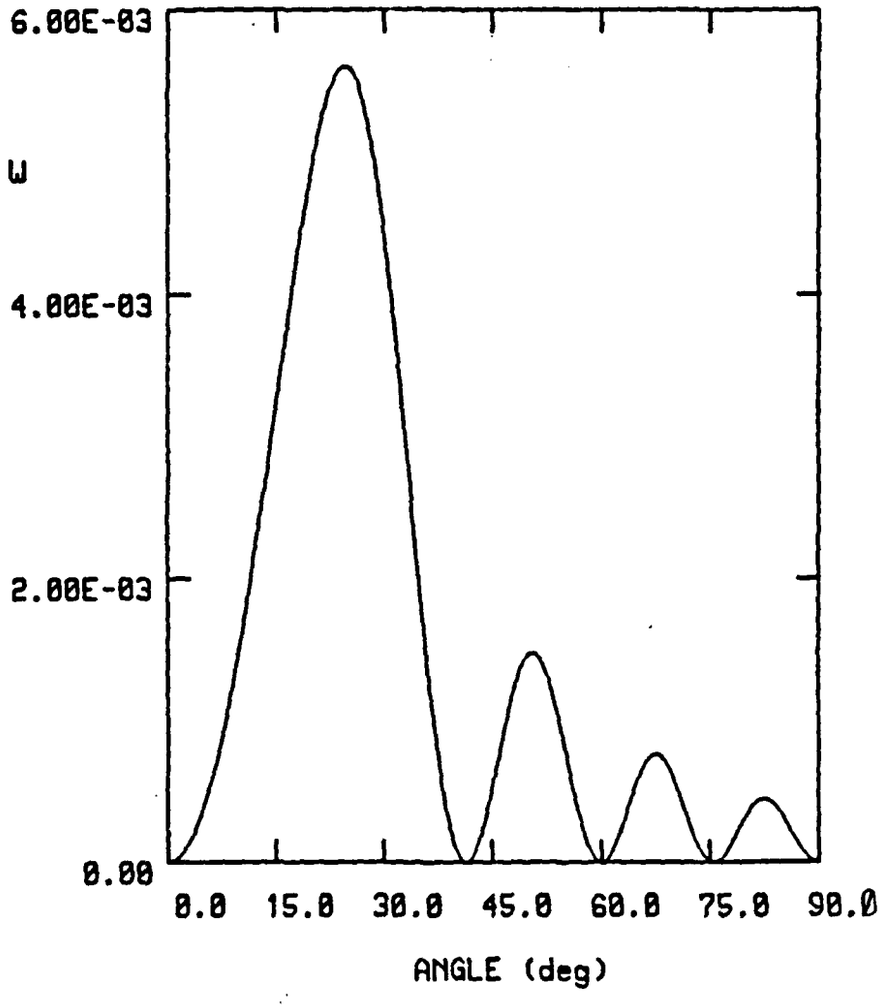

Figure 2. Theoretical Plot of Cerenkov Diffraction Pattern

3. Brief Theory of Transition Radiation

Transition Radiation occurs when a charged particle of constant speed passes through a boundary where the properties of the medium change. Often the boundary is between two different dielectric media, but a dielectric-conductor, dielectric vacuum, or conductor-vacuum interface suffices to produce transition radiation. If the two media have different optical properties, then a charged particle will always produce transition radiation which will also be dependent on the trajectory of the particle and the angle of observation of the radiation. Two cases arise that are of particular interest. First, when a charged particle, initially in vacuo, enters the surface of a pure dielectric or second, a perfect conductor. For either case, the boundary is assumed to be abrupt, that is, variations in the boundary are assumed to be smaller than the wavelength of the emitted radiation. Whereas Cerenkov radiation has a threshold, transition radiation occurs for any constant particle velocity. When a charged particle travelling through a solid, gas or plasma encounters a density change, it will also produce transition radiation [Ref. 7]. Although closely associated with Cerenkov radiation, the properties of transition radiation are quite different. The intensity is strongly dependent on the energy of the charged particle causing the generated spectrum to extend from the microwave to x-ray

region, where the upper limit is proportional to the Lorentz factor, γ, ($\gamma = 1/\sqrt{1-\beta^2}$). Transition radiation is also polarized. In consonance with Cerenkov radiation, transition radiation is angularly dependent and coherence is achieved through charged particle bunching.

Consider a charged point particle crossing from medium 1 to medium 2 with dielectric permittivity ε_1 and ε_2 respectively, see Figure 3, (Figure 2, [Ref. 7]). In crossing this single interface, it is assumed that the path of the particle is normal to the surface. Ginsburg and Frank developed the following equation of the transition radiation intensity per unit frequency for this case [Ref. 8]:

$$\frac{dI_2(\hat{n},\omega)}{d\omega\, d\Omega} = \frac{e^2 v^2 \sqrt{\varepsilon_2} \sin^2\theta_2 \cos^2\theta_2}{\pi^2 c^3}$$

$$\times \left| \frac{(\varepsilon_1-\varepsilon_2)(1-\beta^2\varepsilon_2-\beta\sqrt{\varepsilon_1-\varepsilon_2\sin^2\theta_2})}{(1-\beta^2\varepsilon_2\cos^2\theta_2)(1-\beta\sqrt{\varepsilon_1-\varepsilon_2\sin^2\theta_2})(\varepsilon_1\cos\theta_2+\sqrt{\varepsilon_1\varepsilon_2-\varepsilon_2^2\sin^2\theta_2})} \right|^2$$

When the Cerenkov conditions are satisfied the denominator in the equation becomes zero if ε_2 is purely real which corresponds to a transparent medium. This exemplifies the close association between Cerenkov and transition radiation [Ref. 9]. In the case where medium 1 is a vacuum, $\varepsilon_1 = 1$, then this equation simplifies to [Ref. 10]:

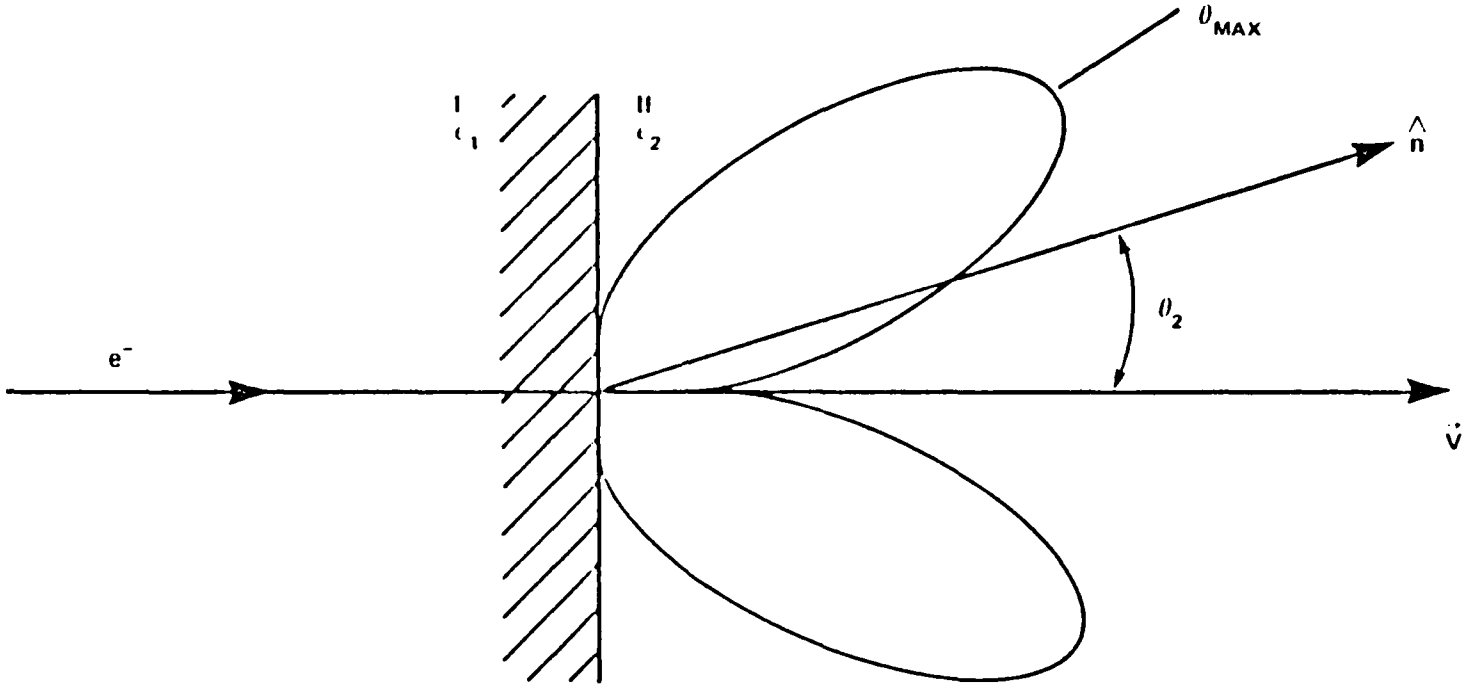

NOTES. MEDIUM I AND MEDIUM II HAVE DIELECTRIC FUNCTIONS ϵ_1 AND ϵ_2.
THE DIRECTION OF OBSERVATION IS $\hat{n}$ AT AN ANGLE θ_2 WRT THE PARTICLE VELOCITY $\dot{V}$.
NOT SHOWN IS THE BACKWARD TRANSITION RADIATION WHICH HAS A SIMILAR INTENSITY DISTRIBUTION.

FIGURE 3. TRANSITION RADIATION PRODUCED IN THE FORWARD DIRECTION AT AN INTERFACE.

$$\frac{dI_1}{d\omega d\Omega} = \frac{e^2\beta^2}{\pi^2 c} \frac{\sin^2\theta_1}{(1-\beta^2\cos^2\theta_1)^2} \left|\frac{\sqrt{\varepsilon}_2-1}{\sqrt{\varepsilon}_2+1}\right|^2$$

According to Rule and Fiorito [Ref. 7], transition radiation has a strong dependence on the energy of the charged particle which caused the radiation. This energy dependence appears in the angular dependence of the transition radiation intensity, in the frequency dependence, and in the total transition radiation intensity [Ref. 7]. It is this property which differs significantly from that of Cerenkov radiation where the dependence is primarily on the particle velocity.

4. Brief Theory on Diffraction Transition Radiation

Diffraction transition radiation is closely associated with transition radiation. It is created by a charged particle of constant velocity passing through a hole or near an interface between two media which posses different dielectric constants. This radiation is known to occur in linear accelerators when bunched charges lose energy in transiting the radio frequency accelerating modules and is known as "beam loading" [Ref. 7].

Although much research has been done on diffraction transition radiation, it pertains to a single charged particle. Bass and Yakovenko have reviewed several cases of radiation produced by a particle passing obstacles [Ref. 10]. Ter-Mikaelian discusses a charged particle passing through a circular hole [Ref. 2]. The physical aspect of diffraction

transition radiation involves fast particles of constant velocity, the Huygens principle and scattering of pseudo-photons. In this discussion, fast particles refers to the field of the particle becoming equal to a set of flat waves. In the development by Panofsky and Phillips [Ref. 11], the moving charge is surrounded by electric and magnetic fields, which have the form of a pulse for an observer near the trajectory. This pulse may be considered as a superposition of plane waves by Fourier transformation and each frequency component may in turn interact with the external system near the electron path. The approach is similar to the calculation of light wave diffraction using Huygens principle as developed by Ter-Mikaelian and Khachatrian. This method is valid if the wavelength, λ, incident on the hole is small compared to the radius of the hole. Additionally, deflection angles of the propagating wave's initial direction must be small (that is, only small deviations from the laws of geometrical optics can be tolerated). This should satisfy the following two conditions: the wavelength is much smaller than the hole radius and the angle of the produced radiation relative to the beam is much smaller than 1. These two conditions should be maintained provided the radiation process is viewed as scattering of pseudo-photons. Using the Huygens principle to calculate the radiation introduces peculiarities because the charged particle field depends on the distance along the path. Ter-Mikaelian concludes that

diffraction radiation of frequency, ω, will occur if the wavelength divided by the hole radius is greater than or approximately equal to the inverse of the Lorentz factor ($\frac{\lambda}{a} \gtrsim \gamma^{-1}$). The better this condition is fulfilled the greater will be the intensity of the diffraction radiation. Given a particle velocity v passing through a hole of radius a with R representing an off axis distance as in Figure 4 (Figure 10, [Ref. 7]), $\frac{\gamma v}{\omega} >> a$ and $R << a$, Ter-Mikaelian developed an expression for the number of quanta of frequency ω radiated in the range $d\theta$ about the observation angle θ by one electron which is (Equation (31.15), [Ref. 2]):

$$N\, d\omega d\theta \simeq \frac{1}{137\pi} \frac{\theta^3 d\theta}{(\gamma^{-2}+\theta^2)^2}[J_o^2(qa) + (\frac{R}{a})^2 J_1(qa)]\frac{d\omega}{\omega} \qquad (4)$$

where the factor q in the argument of the Bessel functions $J_o(qa)$ and $J_1(qa)$ is the projection of the wave vector $\vec{k}$ into the plane z = 0 of Figure 4, i.e., $q = k \sin\theta$, and the angle of $\vec{q}$ with respect to the x-axis is ψ [Ref. 7:p. 28]. The θ-dependence of diffraction radiation is characteristic of that for transition radiation except for the hole in the screen which causes the Bessel functions to arise. Rule and Fiorito state that coherent diffraction radiation should be produced if the separation of the bunches in the particle beam are on the order of or smaller than the wavelength. Diffraction radiation will be produced by a beam at wavelengths satisfying the relation

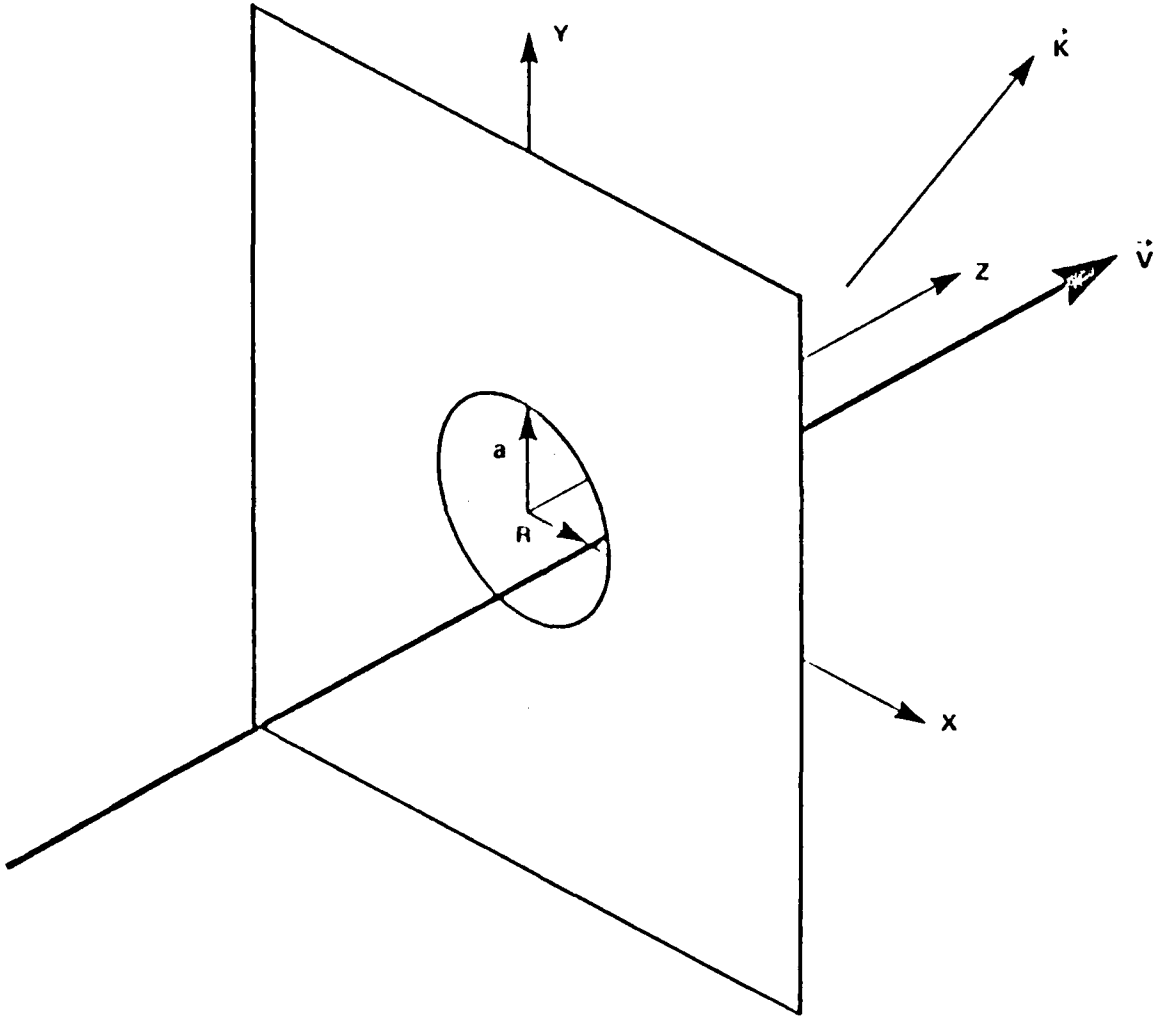

FIGURE 4. DIFFRACTION TRANSITION RADIATION OF WAVE VECTOR $\dot{K}$ PRODUCED BY A PARTICLE OF VELOCITY $\dot{V}$ TRANSITING A DISTANCE R FROM THE CENTER OF A HOLE OF RADIUS a IN A SCREEN.

$$n_b^{-1/3} \lesssim \lambda$$

where n_b is the beam density. The more this relation is satisfied the more that both transition and diffraction radiation will be enhanced and the intensity of radiation will become proportional to n_b^2. This coherent behavior has applications in beam diagnostics.

B. PREVIOUS EXPERIMENTS AT NPSAL

All experiments conducted previously have considered only Cerenkov radiation. Bruce provides an excellent summary of the relevant experiments [Ref. 5]. However, in the past experiments, transition and diffraction transition radiation may have been produced by the physical arrangement of the boundary where the beam leaves the accelerator beam pipe through a circular KAPTON aperture and enters air, where the Cerenkov radiation was produced.

C. PURPOSE

The purpose of this experiment has been divided into three areas:

1. It has incorporated suggestions proposed by Bruce [Ref. 5] and Buskirk to further improve confirmation of Equation (1) by improvements in recording data through noise reduction.

2. It was conducted at three energy levels: approximately 96 MeV, approximately 25 MeV and approximately 19 MeV to investigate possible changes in the resulting Cerenkov diffraction pattern.

3. In attempting to reduce noise further in this phase, possible inherent transition radiation was discovered. Further research lead to Reference 7. Thus this experiment will attempt to isolate Cerenkov, transition and diffraction radiation through an empirical analysis of the angular dependence of the generated diffraction pattern.

II. THE EXPERIMENT

A. EXPERIMENTAL SETUP

1. Discussion

The experimental setup is shown in Figures 5-8. This arrangement is very similar to that used by Bruce [Ref. 5]. In the experimental station, also known as the end station, is situated the feedhorn assembly, travelling wave tube (TWT) assembly, and interaction region or finite emission length, L, region, Figure 9, which is determined where electron beam enters air to where the radiation is reflected by a mirror. The feedhorn assembly, Figure 10, consists of an x-band microwave horn antenna, a short piece of x-band waveguide, a microwave to RF converter, and a mounting assembly holding the feedhorn which allows the feedhorn to rotate through an angle to measure the angular dependence of the reflected radiation. The TWT assembly, Figure 11, consists of an x-band TWT amplifier, a 8-10 GHz band bass filter and a crystal detector. The radiation produced signal is transmitted from the feedhorn assembly to the TWT assembly through RG 9/U coaxial cable. The interaction region connection through a wooden support to the feedhorn assembly defines an arc of radius r, which is at a distance large enough to be the far field as discussed in Section I and calculated in Table 1. The feedhorn is aimed

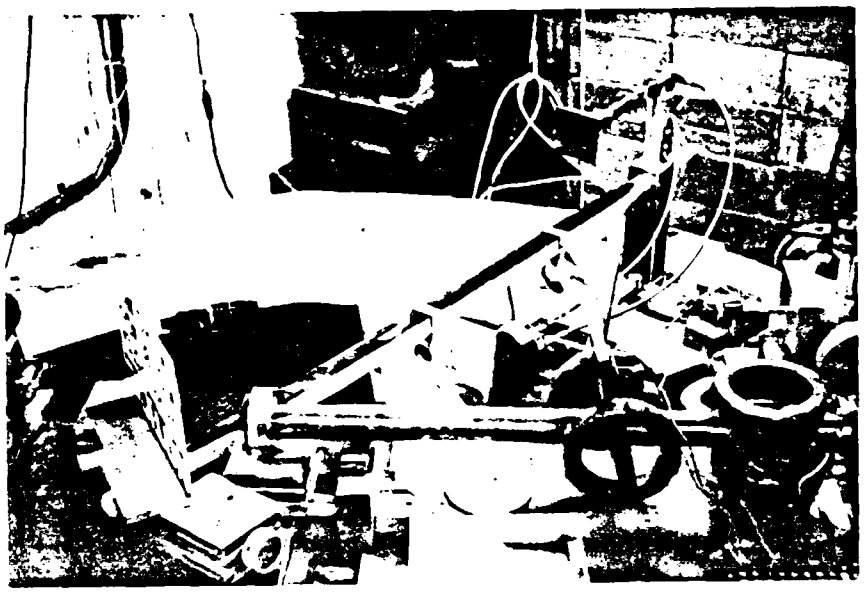

Figure 5. Experimental Setup with Noise Suppressant Material Removed

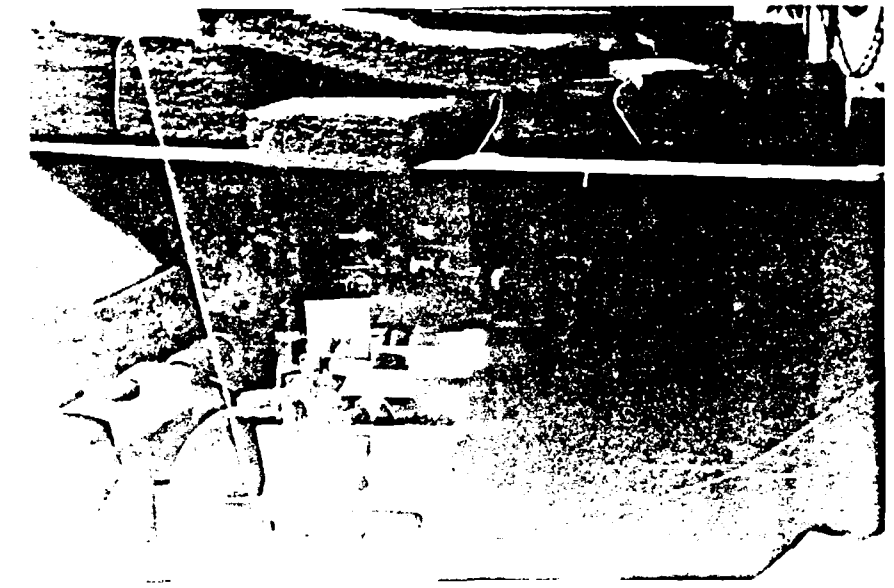

Figure 6. Experimental Setup with TV Monitor While Changing Energy Level

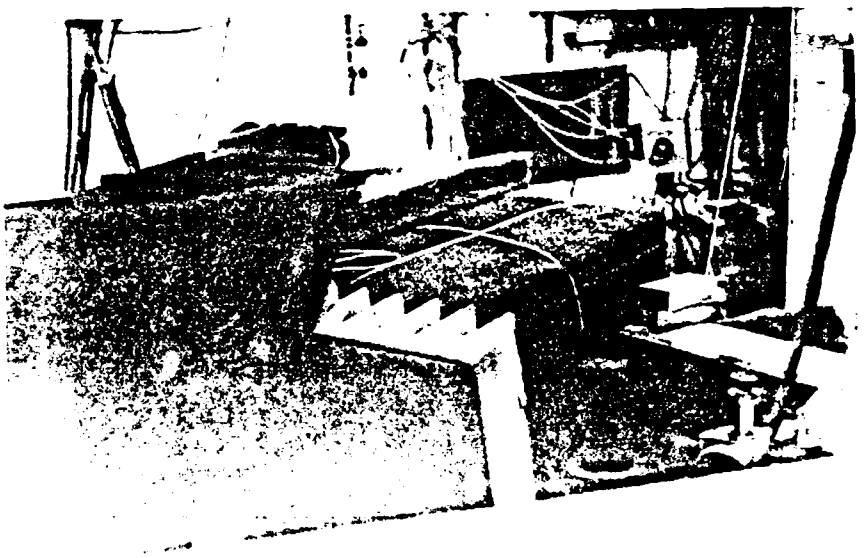

Figure 7. View of Experimental Setup from Behind Showing Absorbent Material

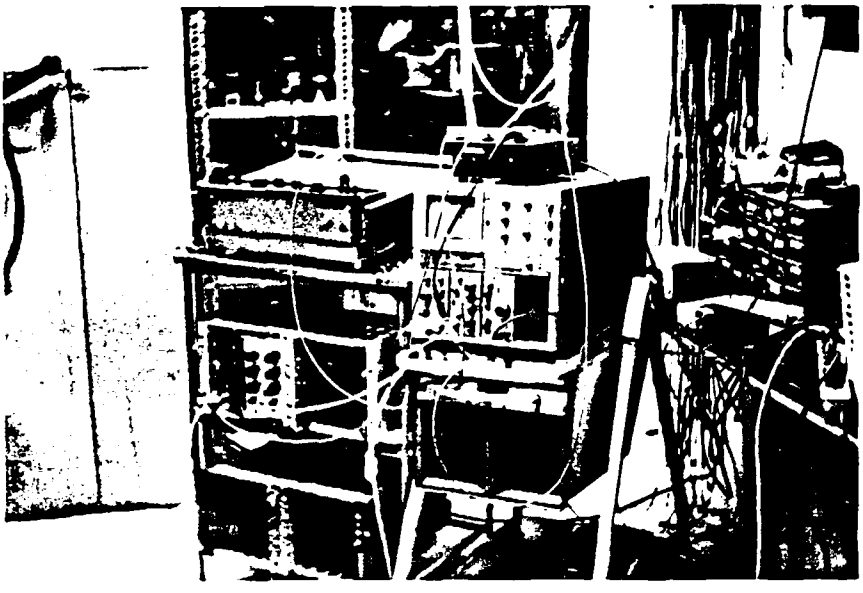

Figure 8. X/Y Recorder, Research Amplifier, Oscilloscope and High Speed Sample and Hold Equipments

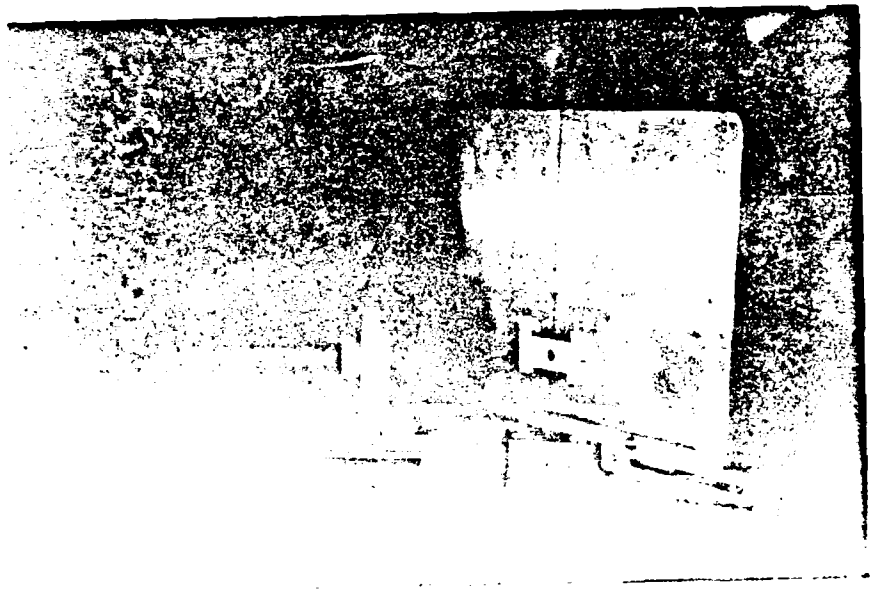

Figure 9. Emission Region Defined by Beam Tube Window and Reflecting Mirror (Reflecting Mirror Has 3/8 Inch Hole with Luminescent Material Taped to Surface Used in Focusing Electron Beam)

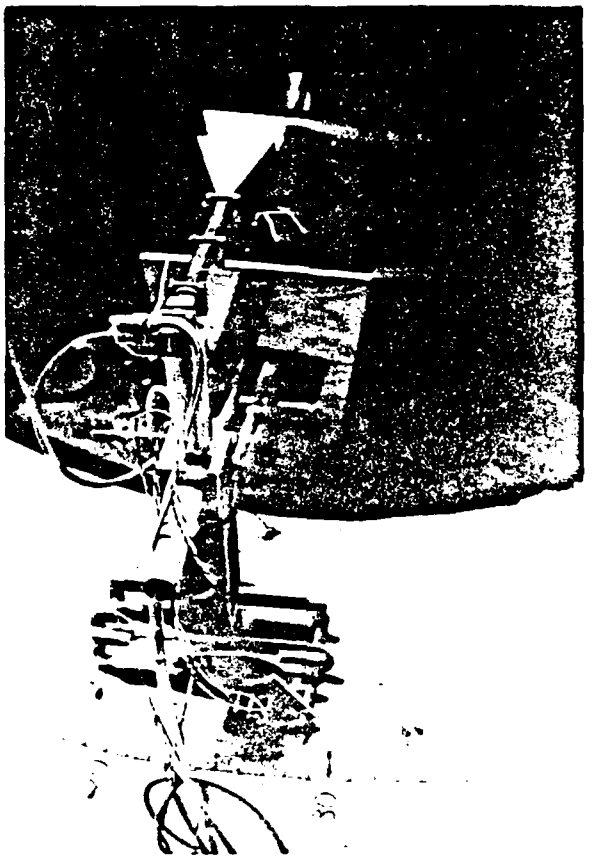

Figure 10. The Feedhorn Assembly

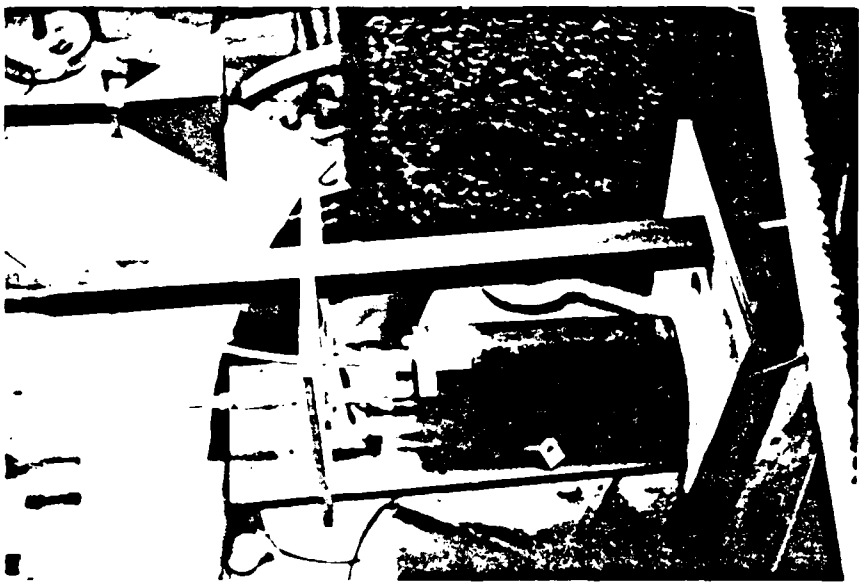

Figure 11. TWT Assembly

at the emission region throughout its arc of travel through careful positioning of the radiation reflecting aluminum mirror. The mirror reflects the electron beam produced Cerenkov, transition and diffraction radiation and establishes the angle relative to the beam path. The intensity of radiation will be a function of this angular dependence. The mirror geometry is illustrated in Figure 13 of Reference 5. Note that it is the radiation reflected from the left hand side of the mirror (looking at the mirror) that is measured in the feedhorn. The microwave signal received at the feedhorn, converted to RF and demodulated by the crystal detector is then transmitted to the control room by triply shielded cable of approximately 25 meters in length. Figures 14, 15 and 16 of Reference 4 and Figure 12 display the attenuation and characteristics of propagation of the feedhorn and TWT assemblies. Upon entering the control room, a signal splitter is used to divert the signal into an oscilloscope for visual reference and to the data collection network. The data collection assembly consists of an amplifier and an integrated circuit high speed sample and hold network which enables the signal to be recorded by the X/Y recorder. The evolution of the radiation from the electron bunched beam to the X/Y recorder is illustrated in Figure 18 of Reference 5. Appendix B contains changes to equipments used in Reference 5.

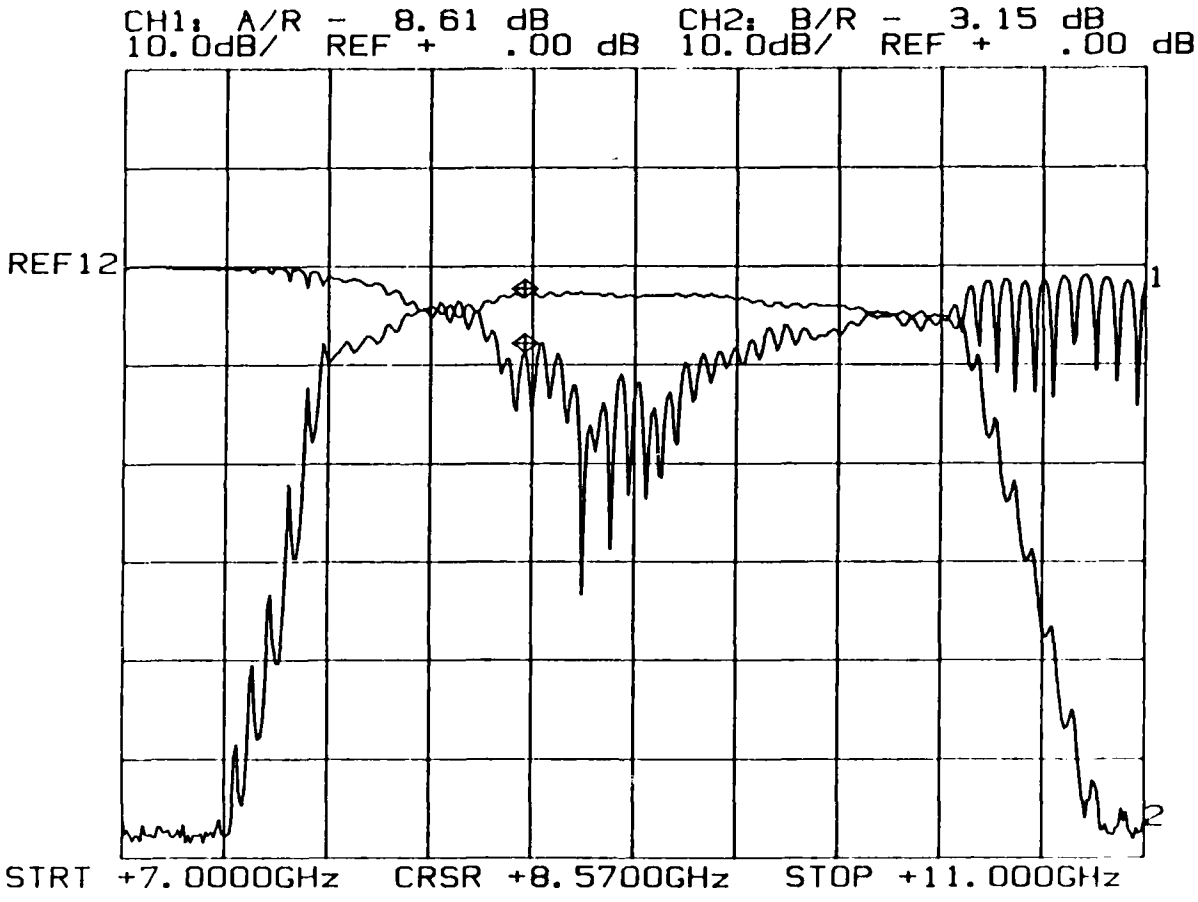

Figure 12. Attenuation Characteristics of Bandpass Filter

2. Problems

The problems encountered in conducting this experiment can be divided into three principal areas. They are: efforts at noise reduction, mirror movement/alignment and voltage/energy fluctuations.

a. Efforts at Noise Reduction

A careful review of Bruce's work [Ref. 5] led to the initial equipment setup. However, upon attempting to identify the low power reflected radiation, it was immediately apparent that there are severe unwanted/stray RF emissions, i.e., noise, masking the desired signal. The cause of the noise is very well documented in Reference 5 and will not be repeated here. The resolution of this problem is quite complex and requires a significant effort, frequently by trial and error. Initially, an 8-10 GHz bandpass filter was inserted into the TWT assembly to preclude the inadvertent amplification of a signal outside the 8-10 GHz range as the experiment concentrates in the third harmonic of the base frequency of the electron beam accelerator, which is at approximately 8.568 GHz. The addition of this bandpass filter was a recommendation from Reference 5. A structure was then built around the interaction region out of microwave absorbing material to isolate the experiment from linear accelerator induced noise and reflections from the walls, celing and floor of the end station. All removable objects in the end station were removed including the mass

spectrograph which was moved away from its previous close proximity as delineated in Reference 5. A metal support which defined the distance to the far field and enabled the feedhorn assembly to measure the angular dependence of the desired signal was changed to a wooden support to reduce reflections into the feedhorn.

The distance, r, which places the feedhorn antenna into the radiation signal far field was changed from 1.6 meters, as used in Reference 5, to 1.12 meters and the emission region L was 14 centimeters. This distance provided results consistent with Reference 5, but the shorter distance increased the signal-to-noise ratio. Buskirk proposed trying yet a shorter distance based on the relation, $r = \frac{2(L \sin\theta)^2}{\lambda}$, to further increase the signal-to-noise ratio. This new r of 0.89 meters did not yield results consistent with previous results. Therefore it was determined that r equalling 0.89 meters put the feedhorn antenna into the signal's near field. Thus the minimum range to the far field was determined to be 1.12 meters which was used throughout the experiment.

Several additional noise suppression suggestions were investigated which were either inconclusive or had no effect on the results. They were grounding of the mirror, using a polarizing filter in front of feedhorn antenna and centering the electron beam through a pipe situated between the mirror and the beam dump to eliminate unwanted radiation. The acid test used to check for noise induced between the

emission region and the far wall in the experiment station was the placing of a piece of microwave absoring material across the interaction region to check for any signals reaching the antenna.

When using the linear accelerator at high energy, obtained with all three klystrons operating, and investigating signals produced by the third harmonic, a wire mesh screen must be installed across the access to the end station from the area of the klystron bank, see Figure 1, to screen out klystron noise which adversely and significantly masks the desired signal.

It was found that using two triply shielded cables as grounding straps connecting the feedhorn assembly to the research amplifier in the control room significantly reduced noise and measurably increased the signal seen on the oscilloscope.

Lastly, it was proposed that the linear accelerator produces microwaves which are propagated down the beam tube. To screen out this effect aluminum foil was placed over the end of the beam tube. This immediately induced transition radiation which significantly altered the Cerenkov signal. This discovery altered the scope of the experiment so as to emphasize the diffraction transition radiation which was mentioned in Reference 7.

b. Mirror Movement and Alignment

The mirror is centered over the pivot point of the feedhorn assembly. The height of the mirror above the

table top must be carefully controlled to allow the pivot mechanism to move freely, but at the same time keeping the mirror in the electron beam. Two lab jacks were used along with a level to position the mirror. The mirror was then optically aligned between the feedhorn antenna and beam tube to determine the hypothetical angle of reflection for the zero angle reference used in the angular dependency function of the intensity diffraction pattern. The problem arises due to the short emission length of 14 centimeters providing a very small area under the microwave absorbent shield in which to work. The optical alignment must be checked each time the electron beam energy is changed or when changing the focus point of the beam. In order to check optical alignment a silvered mirror must be attached to the aluminum mirror and on several occasions the mirror was inadvertently moved. Sometimes it was noted before recording data on a subsequent run, but more often than not only after data was taken which was inconsistent with previously recorded data. There appears to be no final solution to this problem, other than extreme care.

It is desired to operate the feedhorn antenna at the same height and in the horizontal plane of the electron beam to minimize the distance to the far field. It was found that when antenna was so positioned the desired signal was suffering uncontrolled interference. This interference disappeared when positioning antenna four inches higher than electron beam.

The above efforts were rewarded with an improved signal-to-noise ratio which permitted the collection of valid data.

c. Current and Energy Fluctuations

Unfortunately there are no clear cut solutions to these problems and they can be most significant. Due to operating peculiarities of NPSAL it is impossible to operate the linear accelerator at the same precise energy level day to day. The nature of this experiment allowed data to be recorded within an energy band and still be valid. Additionally, and equally as difficult, the current varied not only day to day, but run to run on a given day and even within a single run. Once again because it was only the shape of the diffraction pattern obtained that was desired, this problem did not adversely affect this experiment. On several occasions, however, auxiliary equipment colocated with NPSAL caused such a current drain, that the electron beam would be completely lost momentarily, adversely affecting data collection. Also, much of the so-called fine structure noted in the data can be directly attributed to minor current fluctuations which can not be prevented.

B. DATA COLLECTION

The method of data collection used in this experiment was developed by Bruce [Ref. 5]. The significant improvement which this method provided was the plotting of smooth data

on an X/Y recorder which was possible through the incorporation of a high speed sample and hold integrated circuit (Figure 17, [Ref. 5]).

This experiment was conducted at three energy levels as previously stated and depending on which aspect of the produced radiation was being investigated, determined what equipments were used. The only changes in all three phases involved modifications within the finite emission length as defined by the end of beam tube and aluminum reflecting mirror. Data collection required the use of a metallic mirror because of the two problems which were cited in Reference 5: (1) the study of the first lobe (strongest) of the radiation produced diffraction pattern would require moving feedhorn antenna through the electron beam; and (2) without a mirror it is not possible to reliably define the finite emission length. The differences between the various phases of this experiment involved using a solid aluminum mirror or a similar mirror with a 3/8 inch hole on which was focused the electron beam, see Figures 9 and 13. The hole was put into a mirror to investigate whether this change affected the diffraction pattern. Over the beam tube was placed a solid aluminum plate, no plate, or a series of aluminum plates with different holes drilled as shown in Figure 14. The hole sizes were one inch, 3/4 inch, 1/2 inch and 1/4 inch.

The radiation data collected during the experiment are shown in Figures 15-31. In all cases, L was fixed at 14

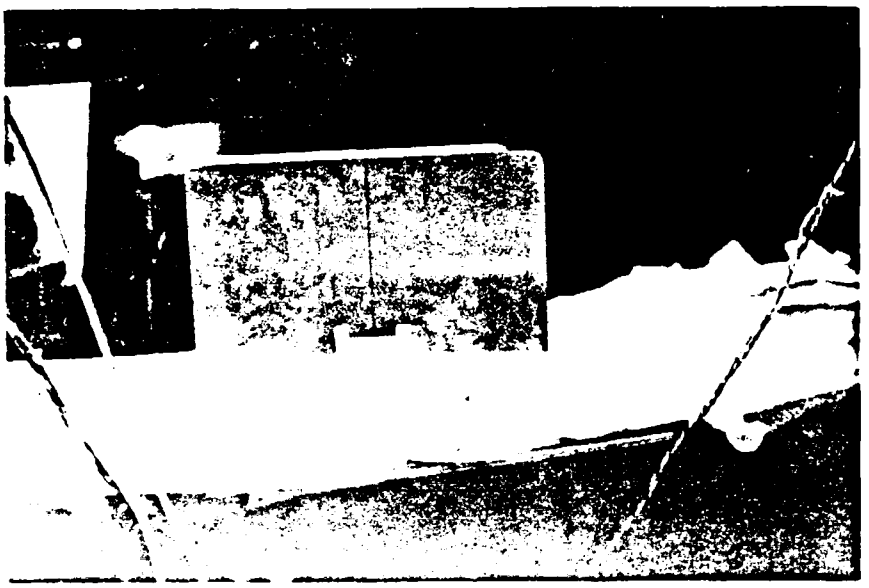

Figure 13. Reflecting Mirror without Hole

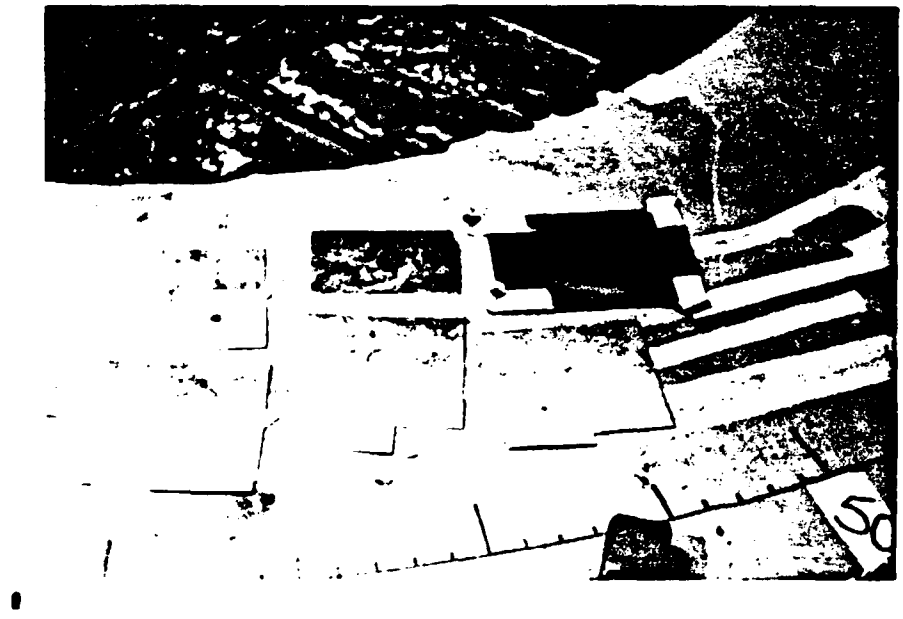

Figure 14. Metal Plates and Optical Mirror.
Upper Row l-r: 1/2 inch hole, solid plate, optical mirror
Lower Row l-r: 3/4 inch hole, 1 inch hole 1/4 inch hole

centimeters and r was set at 1.12 meters. The angular scale along the bottom of the plot displays the relative angle to the beam reflected off the mirror and its range is approximately zero to sixty degrees. The scale along the side is a measure of intensity, W, in arbitrary units.

III. RESULTS AND CONCLUSIONS

A. RESULTS

The most significant aspect of this experiment is that the only way to distinguish between Cerenkov, transition and diffraction transition radiations is through an analysis of their functional dependence in the angular distribution of the diffraction pattern. All three radiations are associated with a single particle or beam bunch moving at a constant velocity. Also, if the boundary (KAPTON window or metal plate) is perpendicular to the electron beam, then all three radiations will have the electric field in the plane of the beam vector and the observer, and the magnetic field will be perpendicular to the plane of the beam vector and the observer. According to Neighbours and Buskirk, Cerenkov radiation will merge into transition radiation by diffraction for a finite path [Ref. 3]. Furthermore, there are no absolute boundaries between Cerenkov, transition and diffraction transition radiation. This experiment attempts an empirical separation of the three radiations through changes generated in the angular dependence of the diffraction pattern. Combinations of Cerenkov, transition and diffraction transition radiation data are shown in Figures 15-31.

In reading Figures 15-31, it should be noted that the zero angle could have as much as a five degree error because

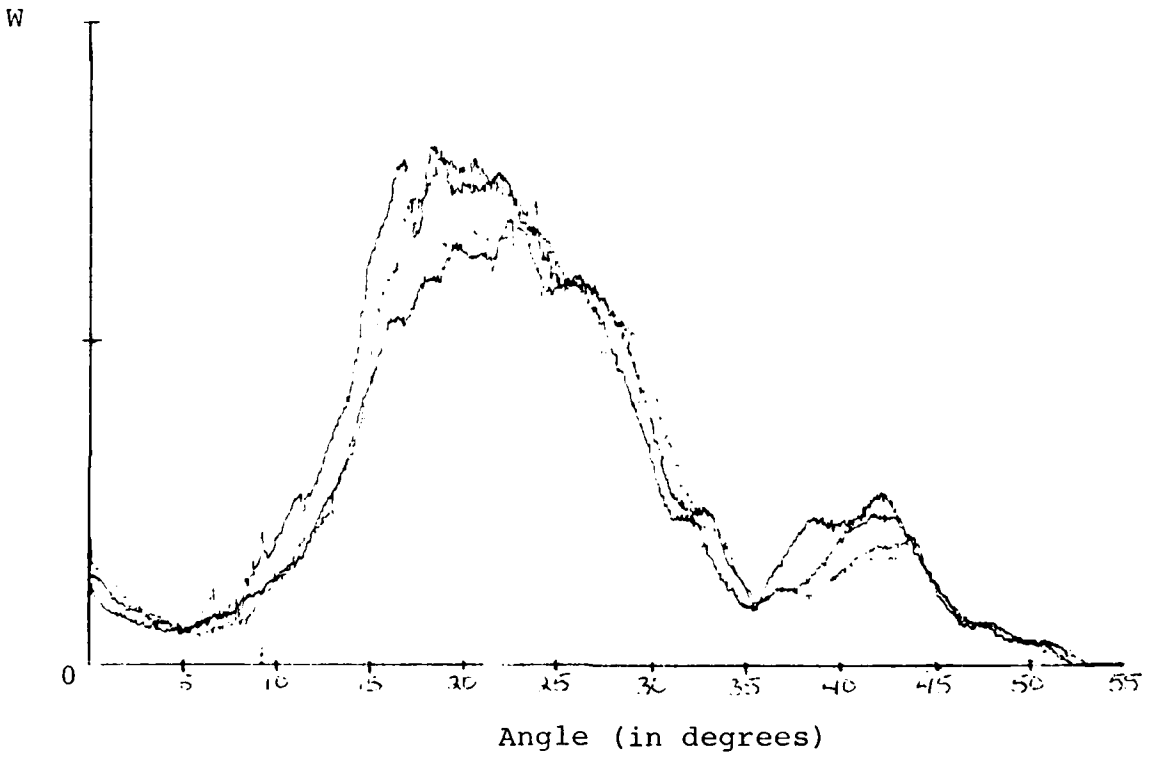

Figure 15. Experimental Configuration at 96 MeV with no Metal Plate Covering Beam Window and Beam Focused at Reflecting Mirror without a Hole

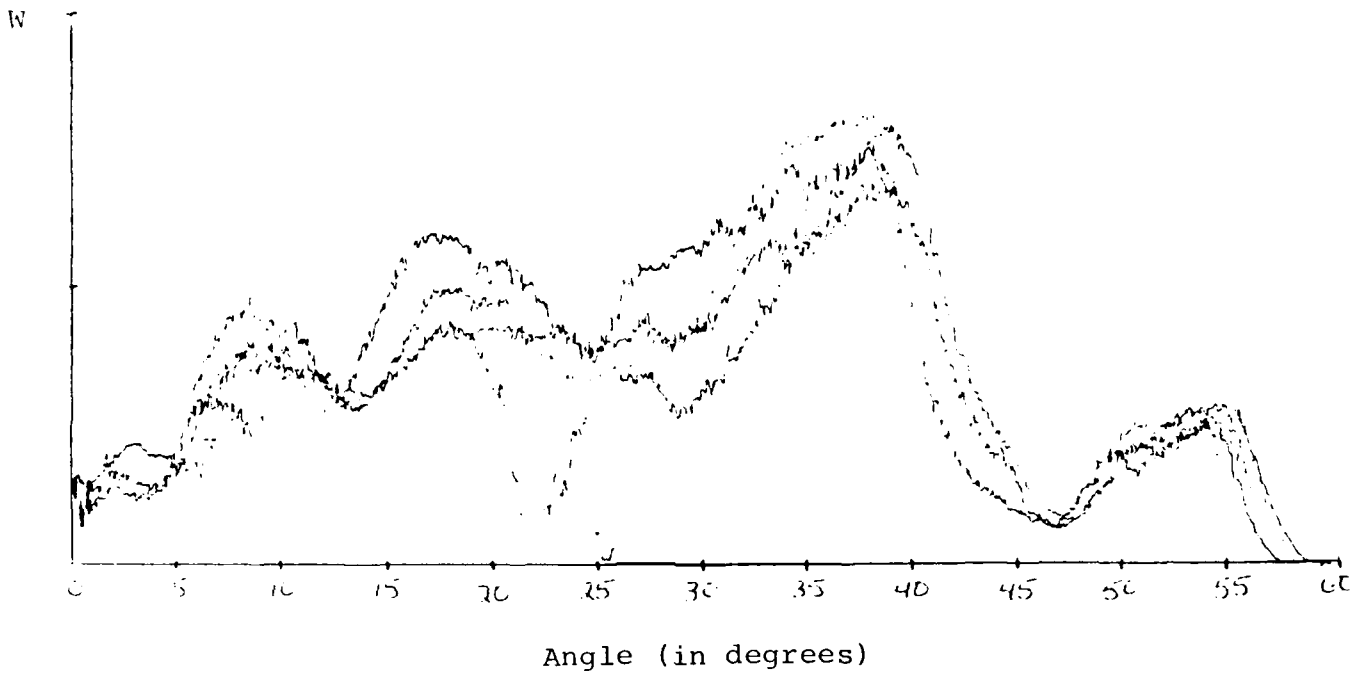

Figure 16. Experimental Configuration at 96 MeV with no Metal Plate Covering Beam Window and Beam Focused on Reflecting Mirror with a 3/8 Inch Hole

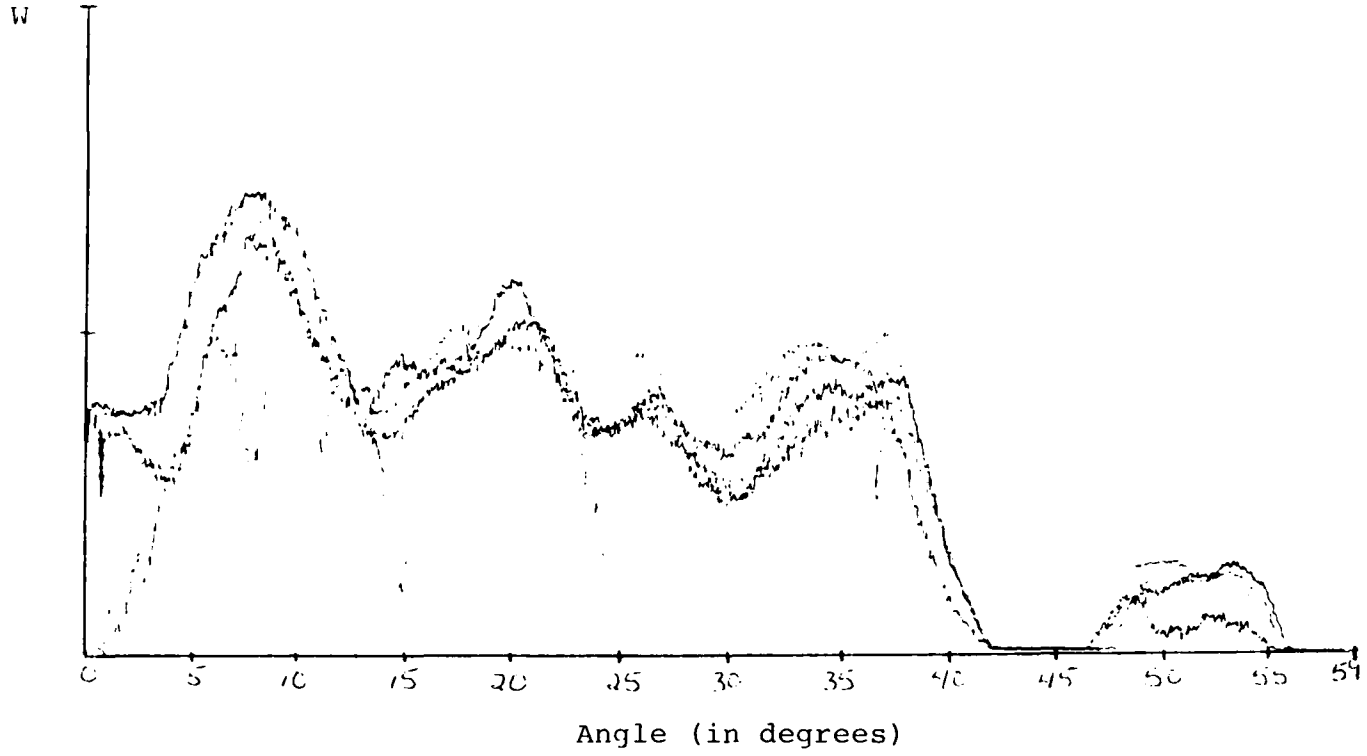

Figure 17. Experimental Configuration at 25 MeV with no Metal Plate Covering Beam Window and Beam Focused at Reflecting Mirror with 3/8 Inch Hole

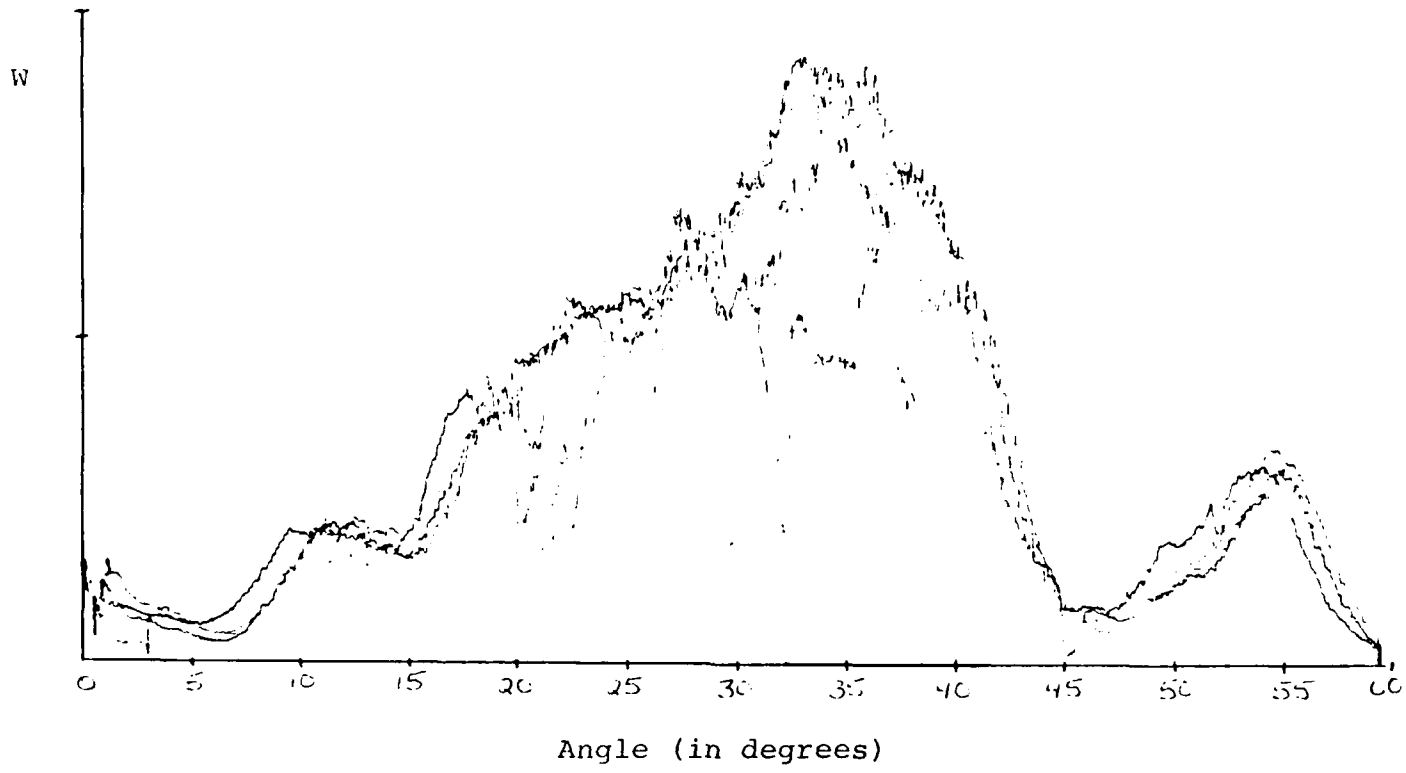

Figure 18. Experimental Configuration at 19 MeV with no Metal Plate Covering Beam Window and Beam Focused at Reflecting Mirror with 3/8 Inch Hole

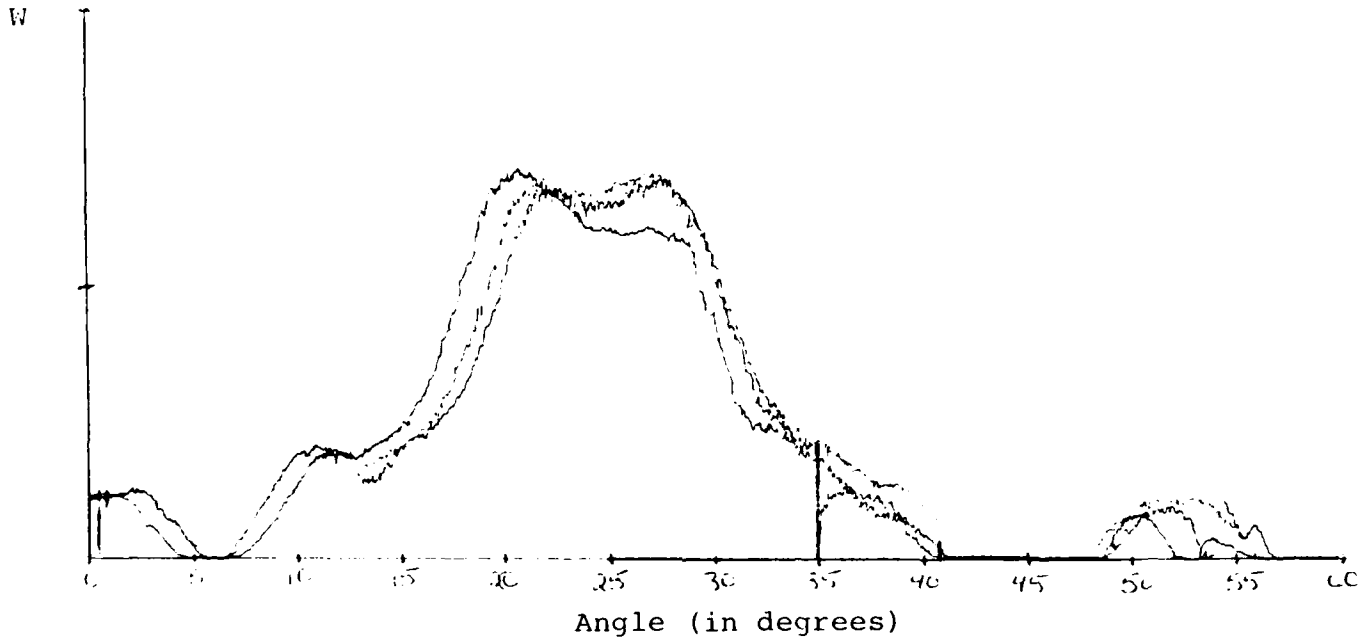

Figure 19. Experimental Configuration at 96 MeV with a Solid Metal Plate Covering Beam Window and Beam Focused at Reflecting Mirrow with 3/8 Inch Hole

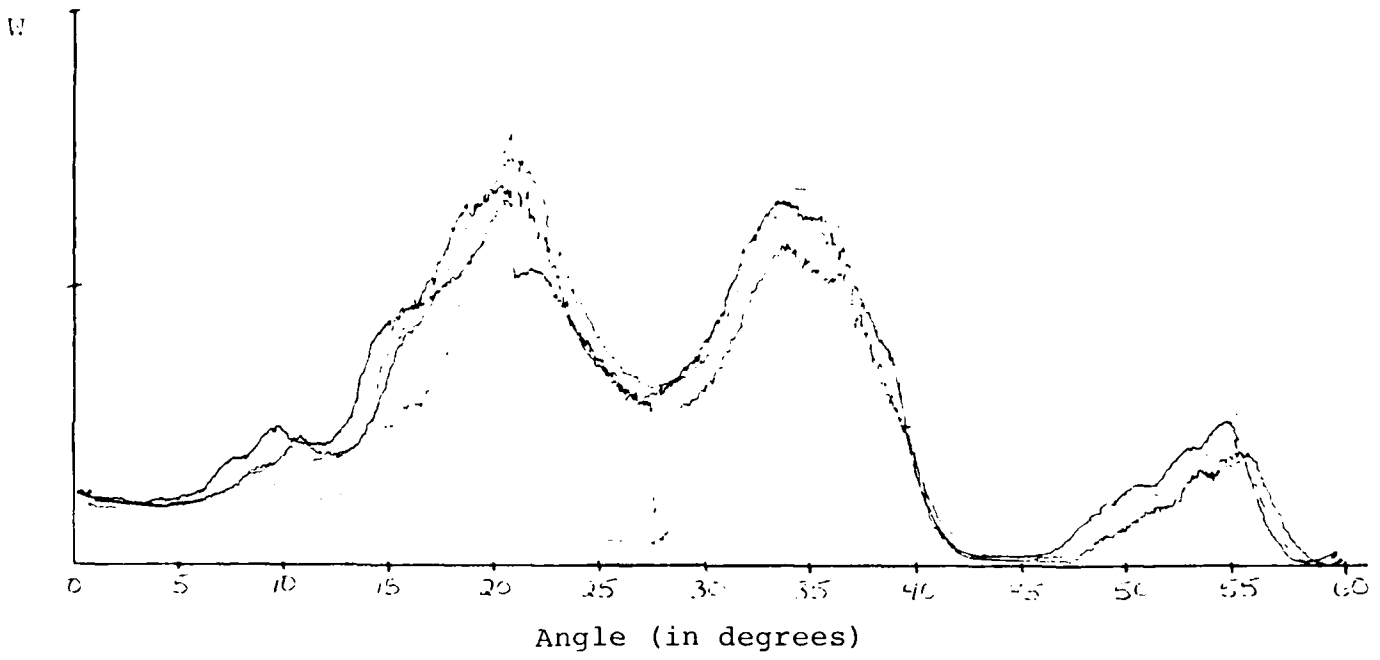

Figure 20. Experimental Configuration at 25 MeV with Solid Metal Plate Covering Beam Window and Beam Focused at Mirror with 3/8 Inch Hole

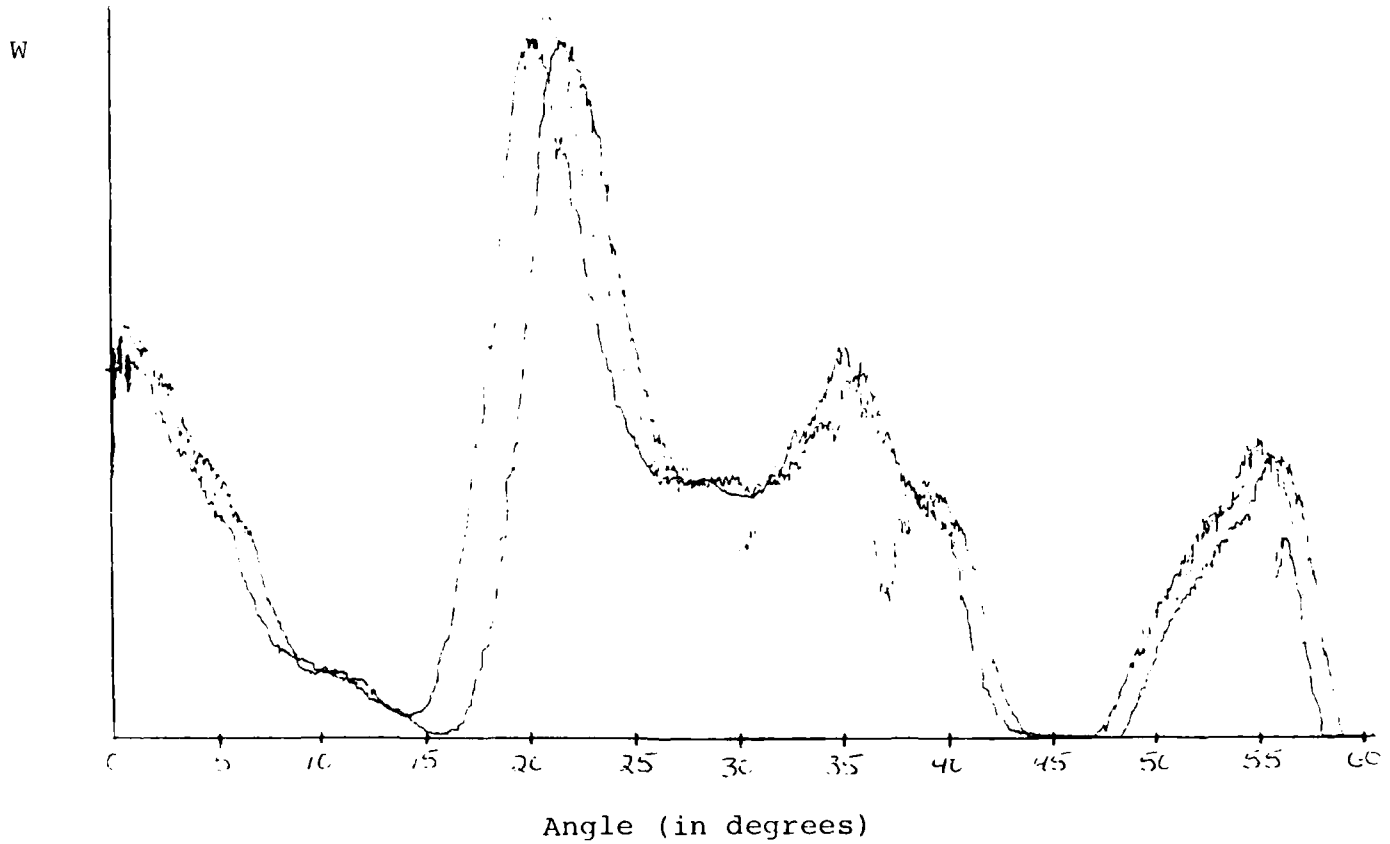

Figure 21. Experimental Configuration at 96 MeV with a One Inch Hole in Metal Plate Centered Over Electron Beam and Beam Focused on Reflecting Mirror with 3/8 Inch Hole

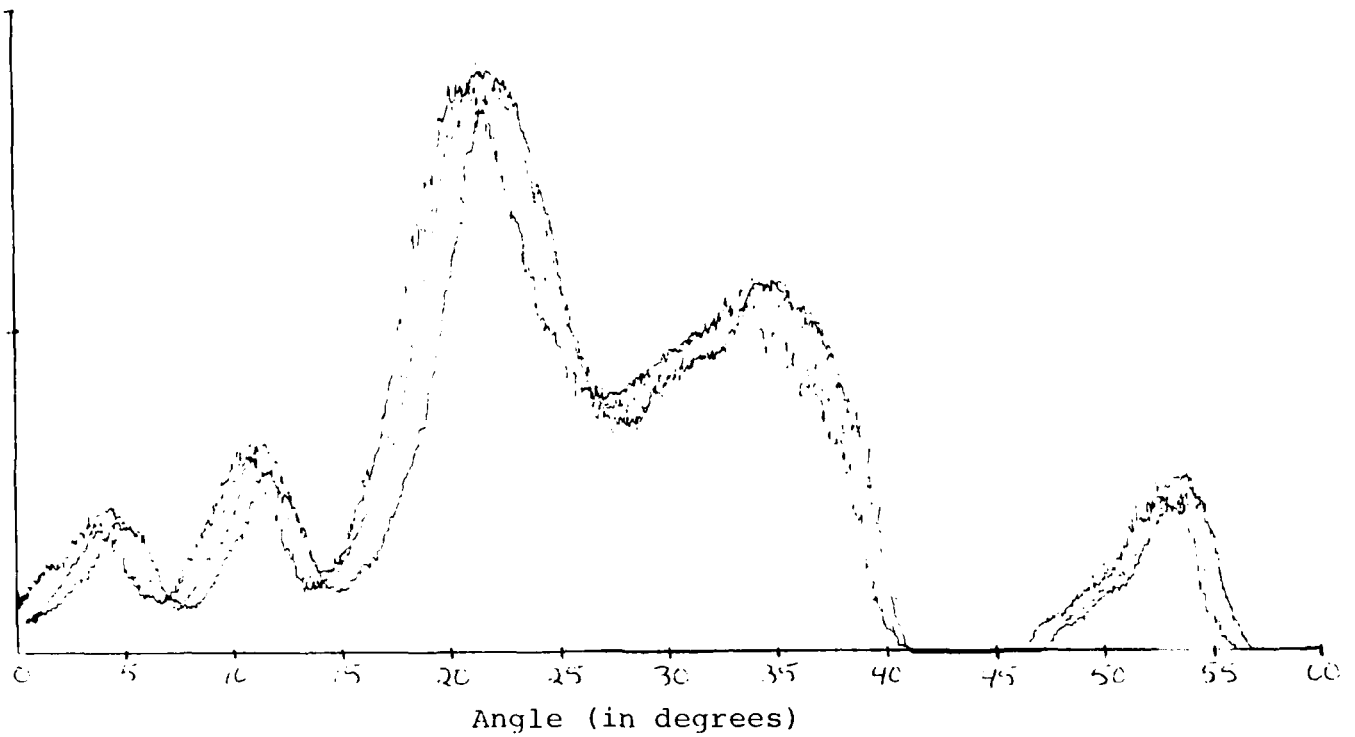

Figure 22. Experimental Configuration at 96 MeV with a 1/4 Inch Hole in Metal Plate Centered Over Beam and Beam Focused at Reflecting Mirror with 3/8 Inch Hole

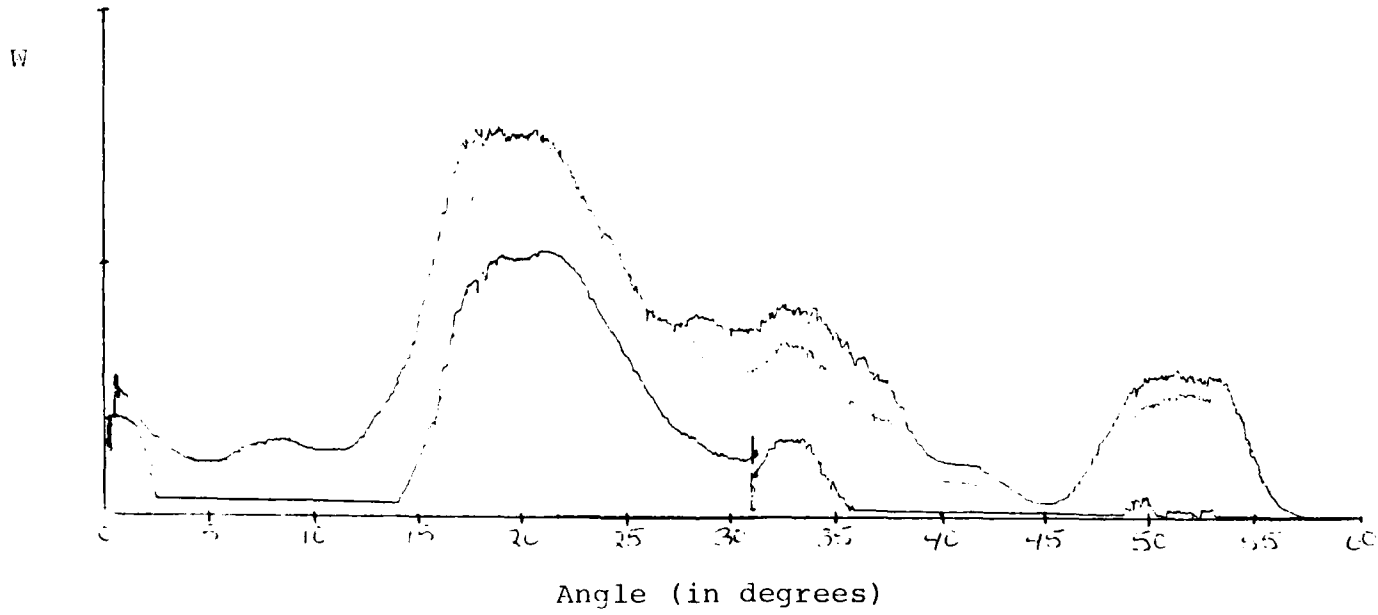

Figure 23. Experimental Configuration at 96 MeV with a 1/2 Inch Hole in Metal Plate Centered Over Beam and Beam Focused at Reflecting Mirror with 3/8 Inch Hole

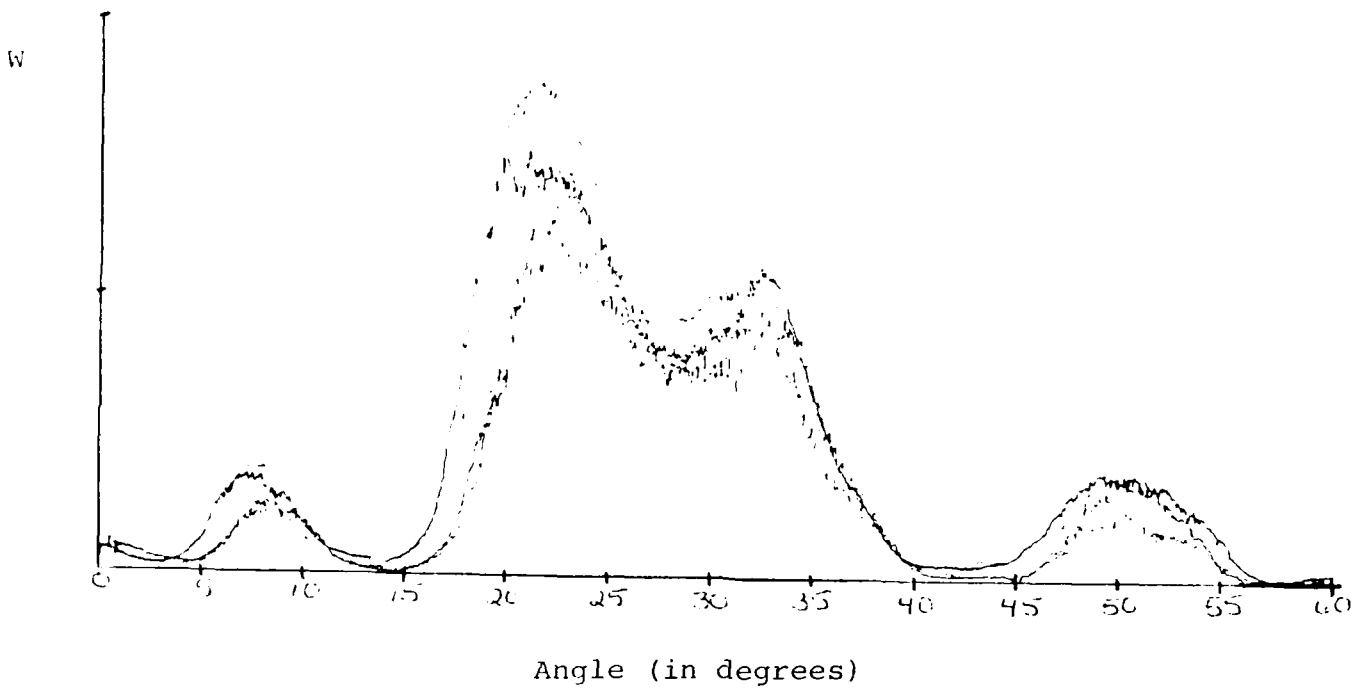

Figure 24. Experimental Configuration at 96 MeV with a 3/4 Inch Hole in Metal Plate Centered Over Beam and Beam Focused at Reflecting Mirror with 3/8 Inch Hole

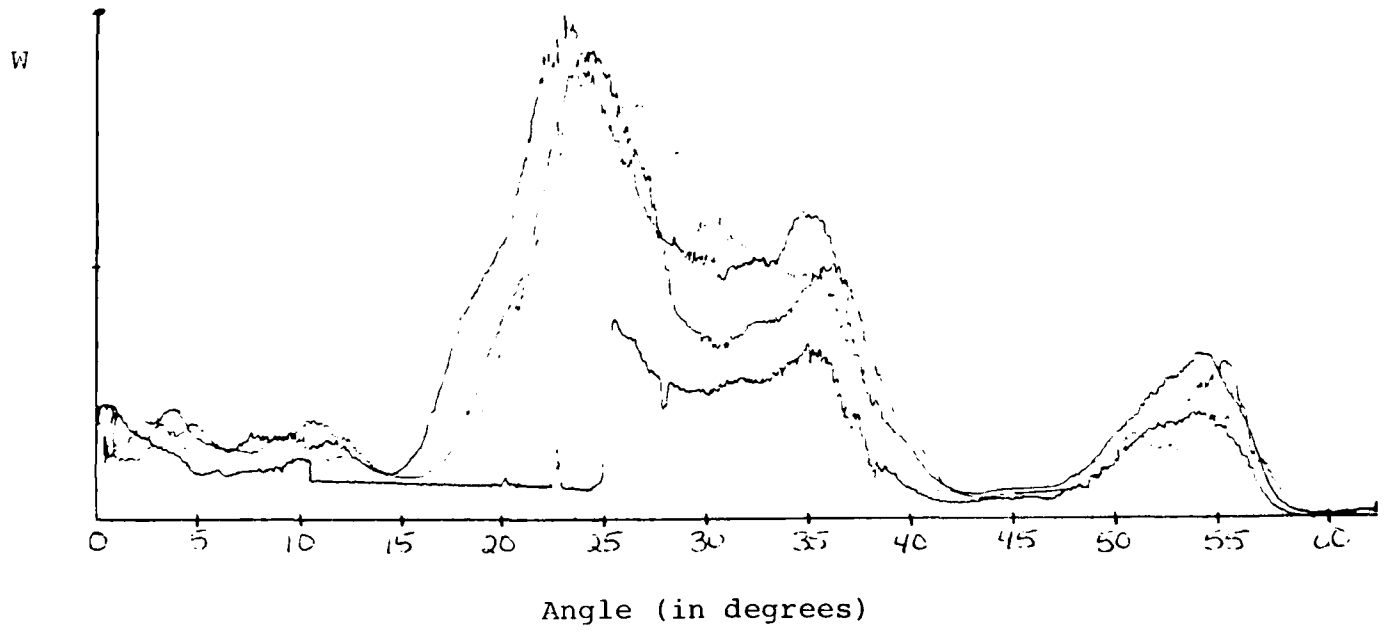

Figure 25. Experimental Configuration at 25 MeV with a One Inch Hole in Metal Plate Centered Over Beam and Beam Focused at Reflecting Mirror with 3/8 Inch Hole

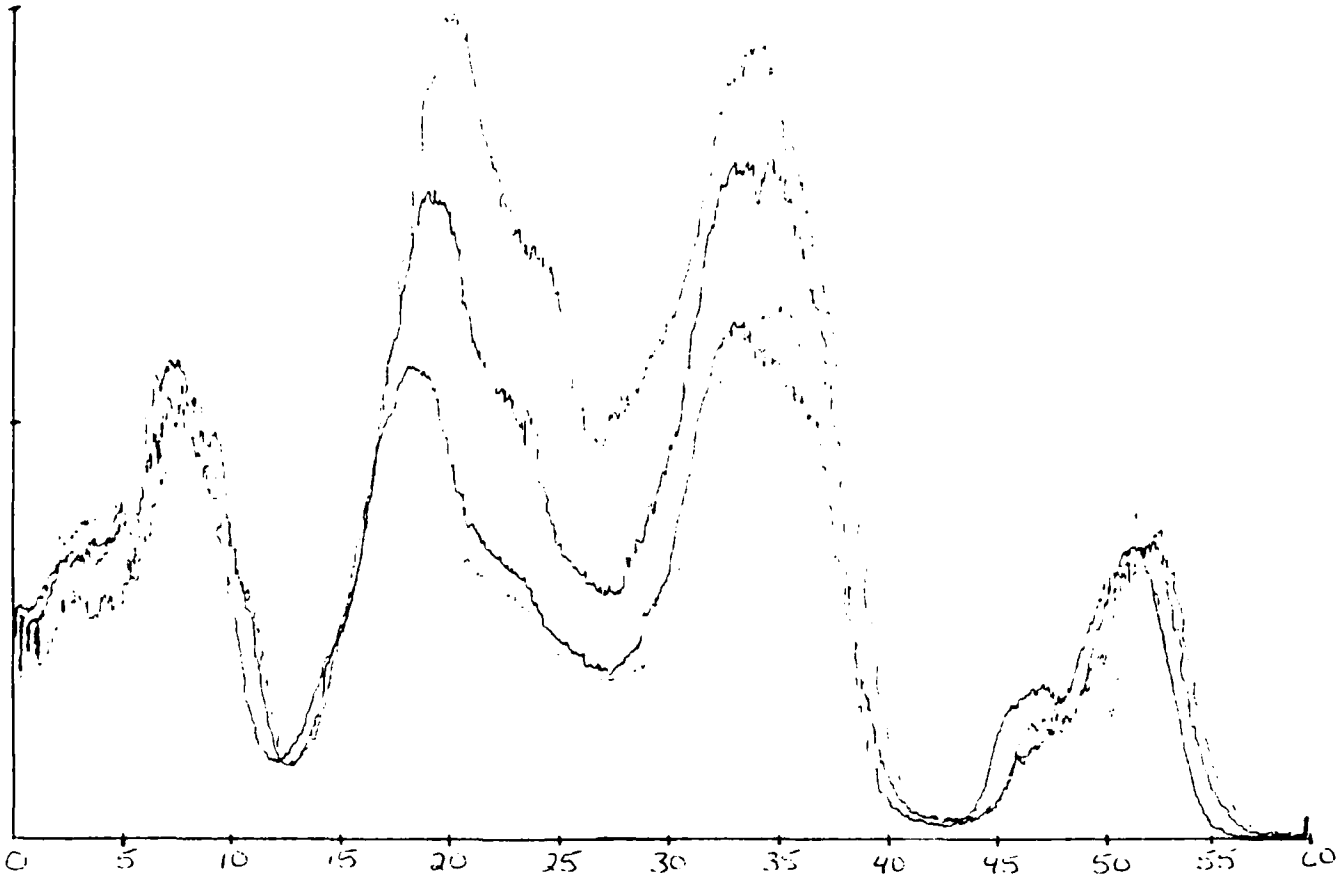

Figure 26. Experimental Configuration at 25 MeV with a 3/4 Inch Hole in Metal Plate Centered Over Beam and Beam Focused at Reflecting Mirror with 3/8 Inch Hole

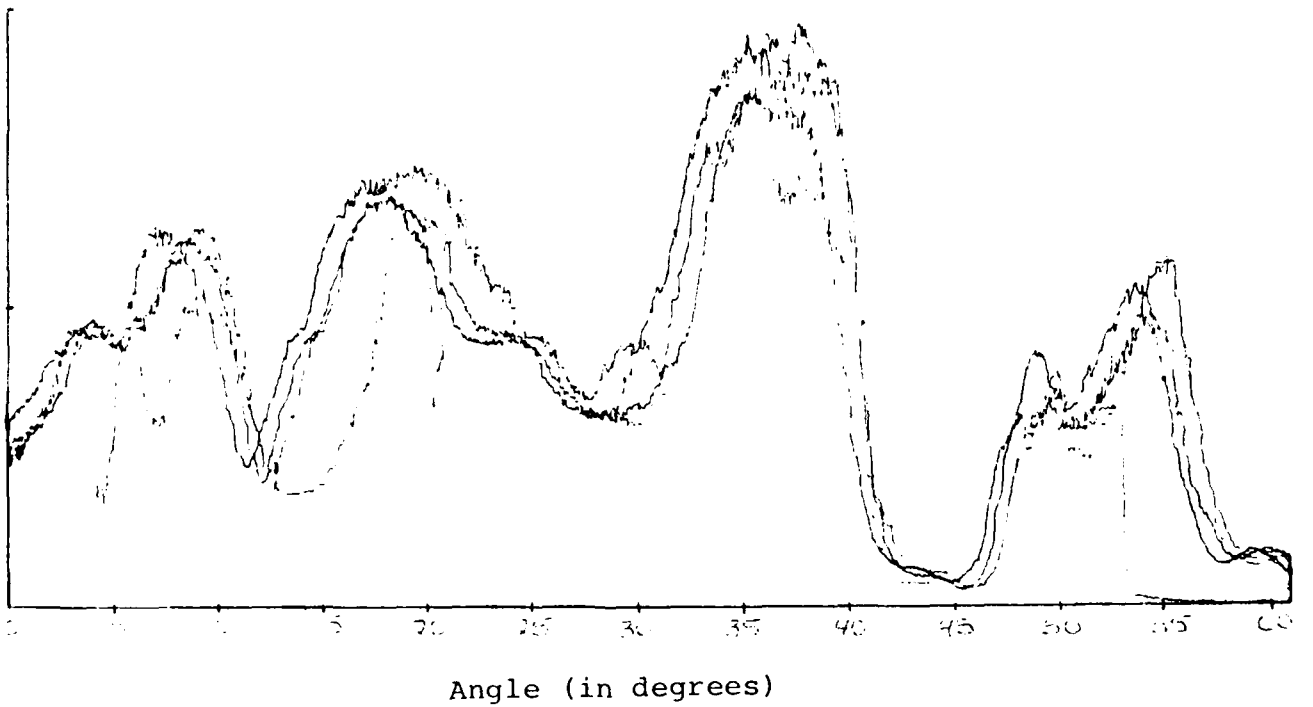

Figure 27. Experimental Configuration at 25 MeV with a 1/2 Inch Hole in Metal Plate Centered Over Beam and Beam Focused at Reflecting Mirror with 3/8 Inch Hole

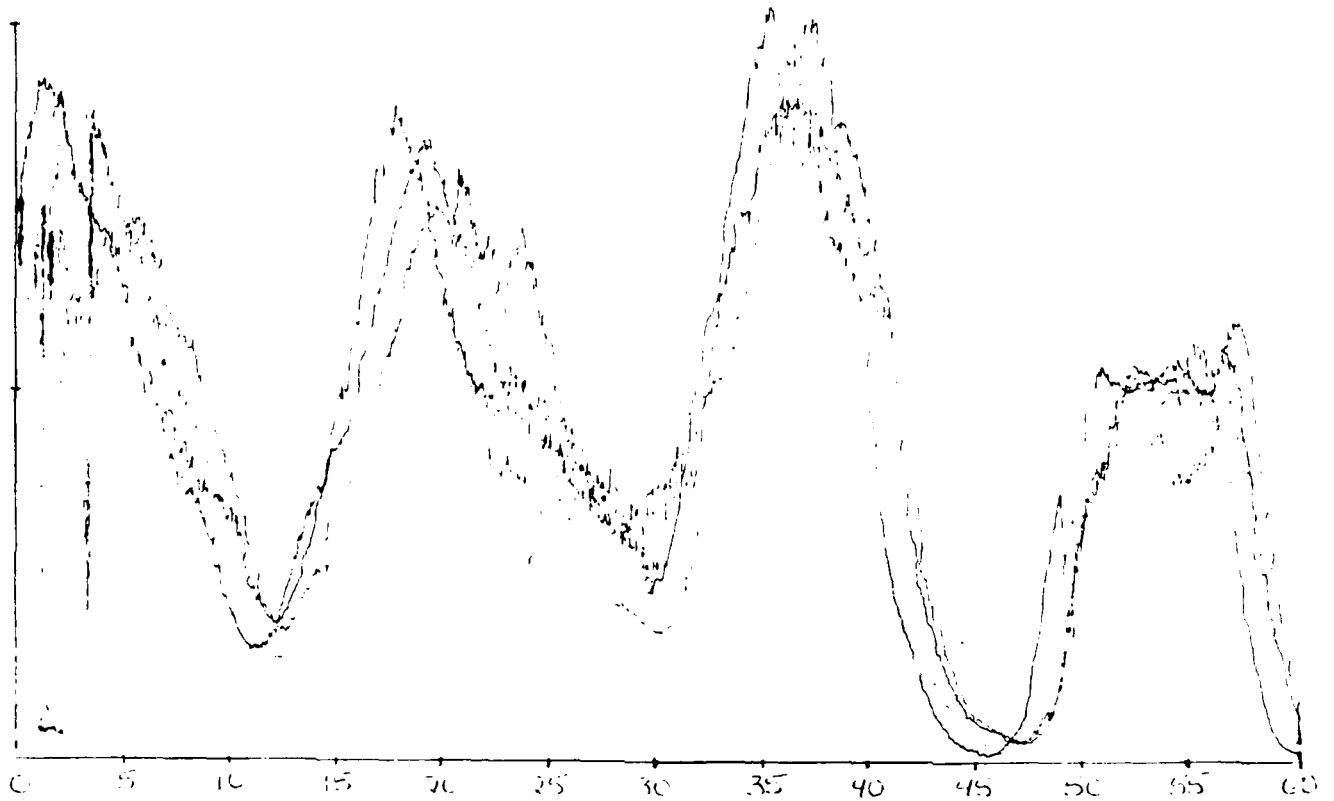

Figure 28. Experimental Configuration at 25 MeV with a 1/4 Inch Hole in Metal Plate Centered Over Beam and Beam Focused at Reflecting Mirror with 3/8 Inch Hole

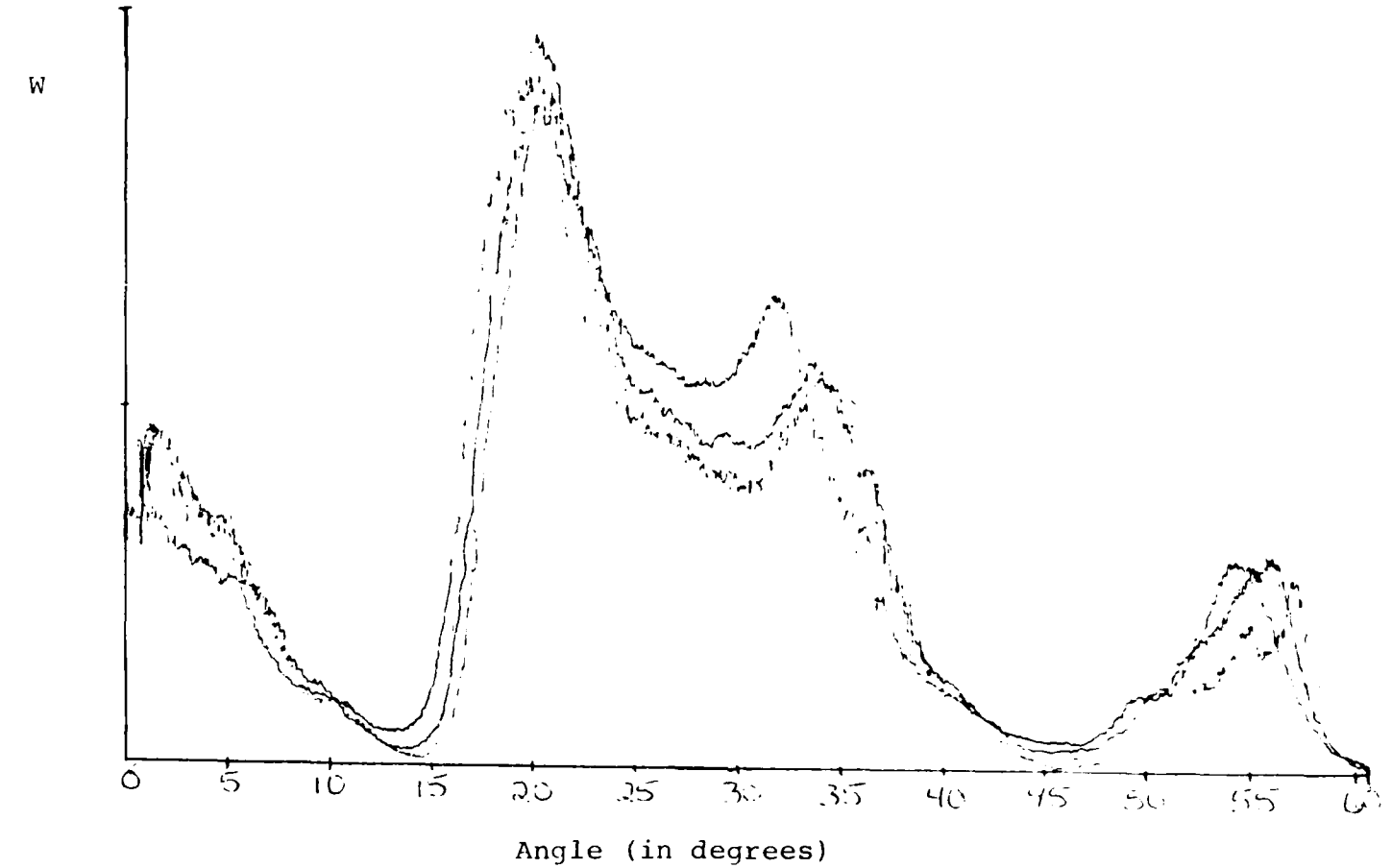

Figure 29. Experimental Configuration at 19 MeV with a One Inch Hole in Metal Plate Centered Over Beam and Beam Focused at Reflecting Mirror with 3/8 Inch Hole

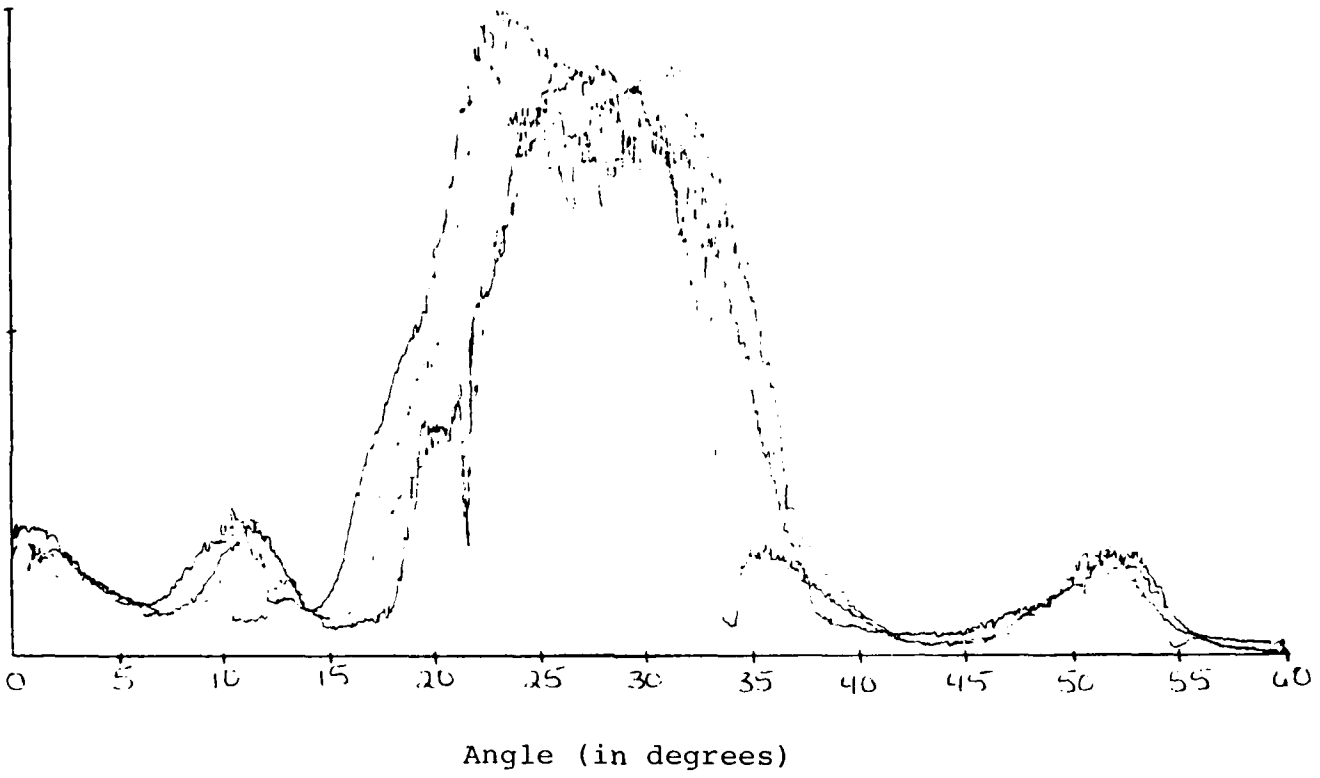

Figure 30. Experimental Configuration at 19 MeV with a 3/4 Inch Hole in Metal Plate Centered Over Beam and Beam Focused at Reflecting Mirror with 3/8 Inch Hole

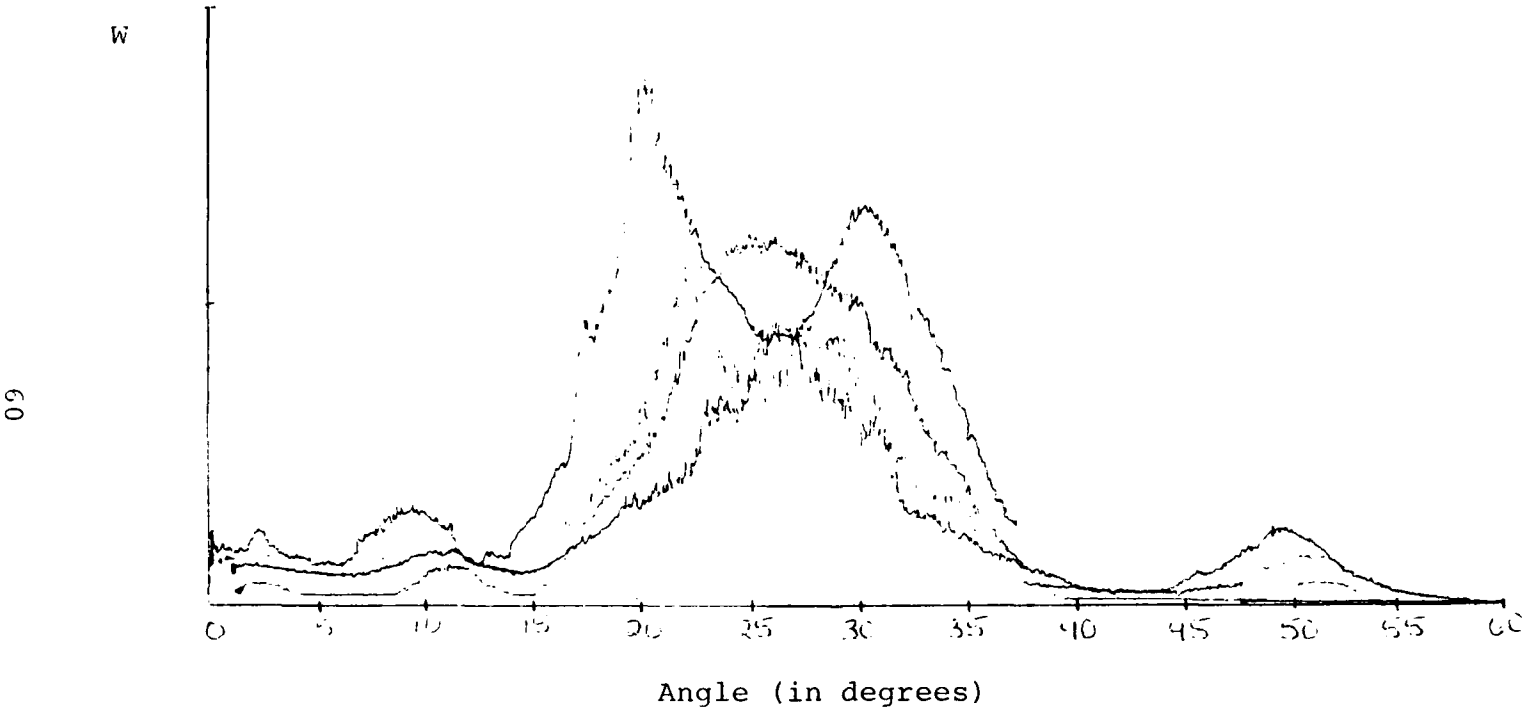

Figure 31. Experimental Configuration at 19 MeV with a 1/2 Inch Hole in Metal Plate Centered Over Beam and Beam Focused at Reflecting Mirror with 3/8 Inch Hole

of its method of measurement discussed earlier and the fact that the potentiometer used in the angular measurement slipped while recording the data. This error can be noted in several of the plots where there appears to be an angular separation between runs within one figure. Each figure represents a minimum of five runs on the X/Y recorder travelling in both directions to obtain accurate and reproducible data. Towards the end of the experiment, the stability of the linear accelerator began to degrade rapidly exemplified with a gradual decay in the beam current level and repeated accelerator interruptions. It is also emphasized that W is measured in arbitrary units.

A theoretical plot of Cerenkov radiation obtained from Neighbours' CERE 10 computer program is shown in Figure 2. The results of this experiment will be broken down into four categories: (1) Comparison of Cerenkov radiation diffraction pattern versus energy, (2) Comparison of transition radiation diffraction pattern versus Cerenkov and diffraction transition radiation diffraction pattern, (3) Effects of hole and hole size in diffraction transition radiation, and (4) Energy dependence of diffraction patterns produced by fixed hole size.

The results presented are based on an empirical analysis of the data. The zero angle plotted in Figures 15-31 is defined by considering an incident photon, moving in the direction of the electron beam being reflected by the mirror

according to the laws of geometric optics. The zero position of the relative angle in these figures is only an estimate due to its imprecise origination (lack of accuracy in the determination of the center line which is sighted optically by the eye). This method was chosen to expand the investigation of angular functional dependence to the maximum limit of the experimental setup (which is approximately 60 degrees in all figures unless otherwise noted) sacrificing precise accuracy of measurements for ease and speed of recording data. The data displayed represents only that portion of the radiation contained in the right hand of the lobe and reflected from the left side of the mirror looking down-beam.

1. Comparison of Cerenkov Radiation Diffraction Pattern Versus Energy

The radiation pattern displayed in Figure 15 resembles the theoretical plot in Figure 2 as to location and relative peak intensities of the first two lobes. In this instance, the reflecting mirror without a hole (Figure 13) was used and the energy level was 95 MeV. Figure 16 is a plot of the diffraction pattern at the same energy, but with a 3/8 inch hole centered on the electron beam in the reflecting mirror. The only correlation with Figure 15 and Figure 2 is its last lobe which is in the same relative angular location. The pattern displayed in Figure 17 resulted from a 25 MeV beam with the 3/8 inch hole in the reflecting mirror. Although the peaks in the diffraction pattern coincide with Figure 16, the intensity level of the first four peaks is

reversed. Upon lowering the energy to 19 MeV, the diffraction pattern of Figure 18 was produced using the 3/8 inch hole in the reflecting mirror. It bears only a faint resemblance to Figure 16, but there are only three peaks readily discernible in Figure 18 and little resemblance to Figures 15 and 17. Data were not taken using the solid reflecting mirror at the two lower energies.

2. Comparison of Transition Radiation Diffraction Pattern Versus Cerenkov and Diffraction Transition Radiation Diffraction Patterns

There are two comparisons made in this section. First, the beam energy will be varied and a solid metal plate is covering the beam tube exit window. Secondly, the beam energy is held constant and the solid metal plate is removed, then inserted over the beam tube window. The significance of this comparison lies in the fact that it is difficult to distinguish the difference in the radiation patterns. Through data taken and displayed in Figures 19 and 20, the sole difference in data should be the result of transition radiation. An aluminum plate 5 5/8 inches by 4 13/16 inches by 0.040 inches thick was inserted flush with the beam tube exit window. This plate will reflect the transition and diffraction transition radiations produced exiting the beam window. The beam window is constructed out of KAPTON, a high strength plastic, in the shape of an 11/16 inch diameter circle in a metal ring. Thus by changing energy levels, changes in transition radiation diffraction

patterns should be noted. Additionally, upon comparison with Figures 16-18, effects due to transition radiation alone should be noted.

The data in Figure 19 were taken at 95 MeV and that in Figure 20 were taken at 25 MeV. Comparing these two figures in which both have the solid metal plate, it is noted that although the intensity is about the same level, the one major lobe in Figure 19 is spread out and divided into two distinct lobes in Figure 20. The lobe on the right side in both figures remained consistent.

The changes in the diffraction pattern between Figures 16 and 19 and between Figures 17 and 20, which is a comparison of the effects of the solid metal plate inserted and removed, is clearly notable and distinct. The only consistency appears to be the last lobe on the right side of the plot and this consistency is in its relative location.

3. Effects of Hole and Hole Size in Diffraction Transition Radiation

The most exciting aspect of this experiment was noting the effects that a hole in a metal plate covering the beam tube exit window and varying its size has in producing diffraction radiation. Although the discussion in Reference 7 applies to a single electron, it appears the diffraction pattern will likewise be generated in a form which for small angles, is proportional to

$$\frac{\theta^3 \, d\theta}{(\gamma^{-2} + \theta^2)^2}$$

The effects of diffraction radiation are displayed upon comparison of Figures 15-31.

At an energy level of about 96 MeV, there is a distinct difference between Figure 19 and Figure 21. The metal plate used in Figure 21 is of the same size and material as that used in Figure 19, except it has a 1 inch hole through which the beam is centered. Also upon comparison of Figure 21 through Figure 24, two groupings become apparent. Figures 22 and 23 (1/4 inch and 1/2 inch holes, respectively) have five distinct intensity peaks, whereas in Figures 21 and 24 (1 inch and 3/4 inch holes, respectively), there are only four distinct peaks. Three apparent cases of correlation occur: (1) The lobes in Figure 22 (1/4 inch hole) and Figure 23 (1/2 inch hole) are coincident after a shift of three degrees with the lobes being located at 4 degrees for lobe 1, 11 degrees for lobe 2, 22.5 degrees for lobe 3, 35 degrees for lobe 4 and 53.5 degrees for lobe 5, (2) Upon comparison of Figures 21 (1 inch hole) with Figure 22 (1/4 inch hole), the extra lobe in Figure 22 occurs at 11 degrees (lobe 2), and (3) Upon comparison of Figure 21 (1 inch hole) with Figure 23 (1/2 inch hole), the extra lobe in Figure 23 occurs at 10 degrees (lobe 2) after a shift of 2 degrees. Apart from these three cases, there appears to be no other cases of correlation. Although the patterns in Figures 21 and 24 are similar, the lobes are not colocated and the peaks of lobes 1, 3 and 4 in Figure 21 are of relative equal

intensity, but in Figure 24, the peaks of lobes 1 and 4 are about 1/3 intensity of lobe 2 and lobe 3 is 2/3 the intensity of lobe 2.

The data in Figures 25-28 were recorded at an energy level of 25 MeV. The effect caused by changing hole diameter is noted at this energy level also, and is demonstrated by the level of intensity in the four peaks of each figure. Upon comparison of the diffraction patterns at this energy, it is evident that they are all different.

After lowering the energy to 19 MeV, the data in Figures 29-31 (1 inch, 3/4 inch and 1/2 inch, respectively) were recorded. The diameter of the hole in the metal plate causes a distinct change in Figure 29, but Figures 30 and 31 are almost identical. The two sets of data were taken at different current levels. The square of the current is directly proportional to the intensity and this explains the variation in the two intensity levels of the main lobe.

4. Energy Dependence of Diffraction Patterns Produced by Fixed Hole Size

The most notable difference demonstrated by the data is in the diffraction patterns produced by the 1/4 inch (Figures 22, 28) and 1/2 inch (Figures 23, 27, 31) diameter holes. At 96 MeV there are 5 distinct lobes in the diffraction pattern, but at 25 MeV and below there are only 4 lobes.

For the 3/4 inch (Figures 24, 26, 30) diameter hole in the metal plate, at both ends of the energy spectrum,

there are only 4 lobes in the diffraction pattern and they are each different in either intensity level and/or functional angular dependence of the lobes.

For the 1 inch (Figures 21, 25, 29) diameter hole, although there is a distinct similarity in the shape of the diffraction pattern, the angular dependence of the lobes is different. The intensity of the peaks, although they appear consistent, are different because they were recorded at different electron beam currents and different gain setting on the X/Y plotter which does not compensate for the apparent consistency.

B. CONCLUSIONS

The scope of this experiment concentrated upon an empirical separation of Cerenkov, transition, and diffraction transition radiation through changes generated in the angular dependence of the diffraction pattern. A comment concerning Cerenkov radiation by itself is also made.

1. The preliminary results obtained, as in Figure 15, while not verifying Equation (2), support its validity. It is speculated that in addition to unaccounted noise, the effects of transition radiation and diffraction transition radiation are always present because of the nature of the exit beam window.

2. The motion of an electron bunch through a hole of varying diameter and varying energy indeed produces differences in the radiative diffraction patterns which must be attributed to diffraction transition radiation. At 96 MeV, three cases of apparent correlation to diffraction transition radiation were identified. When the 1/4 inch hole plate and 1/2 inch hole plate were compared to the one inch hole plate, the second lobe located at about 10.5 degrees

appears to be the effect of diffraction transition radiation. The other case of correlation is between the 1/4 inch hole plate and 1/2 inch hole plate which appear to produce diffraction patterns whose peaks are colocated although of differing intensity.

3. This experiment confirms a methodology to differentiate the effects of Cerenkov, transition and diffraction transition radiation.

4. Although improvements at noise suppression have been made, in order to get more accurate data, further improvements will need to be made.

5. A hole in the reflecting downstream mirror produces a different diffraction pattern than a solid reflecting mirror (see Figures 15 and 16).

6. The theory of diffraction transition radiation exists only for a point charge, and the corresponding theory for radiation from finite size charge bunches is needed for any further comparison to the experiments.

This experiment was conducted with the waveguide feed-horn antenna positioned in a plane 4 inches above that of the electron beam to obtain the most reliable results. It is not understood what caused this aberration from Reference 5, but much time was spent attempting to resolve this problem. Recommendations for future work are contained in Appendix C.

APPENDIX A

OPERATING CHARACTERISTICS OF NPSAL

1. Beam energy varies from approximately 15 MeV through to 100 MeV.
2. Fundamental Bunch Period--2.856 gigahertz.
3. Gaussian bunch parameter--0.0024 meters [Ref. 12].
4. Bunch distance--0.103 meters [Ref. 12].
5. Bunch charge--1.16E-12 Coulomb [Ref. 13].
6. Third Harmonic Frequency--8.568 gigahertz.
7. Wavelength, Third Harmonic Radiation--3.5 centimeters.

APPENDIX B

DESCRIPTION OF EQUIPMENT

The equipment listed here are changes to Appendix A of Reference 5.

Absorbing Hood--This was not used.

Beam Cover--This was not used.

Antennas--The 2 to 18 GHz pyramidal antenna was not used.

Coaxial Cable (RG 9/U) --Only one length of about one meter was used in this experiment which improved the signal-to-noise ratio by about 3 dB.

Tunable YIG Filter (IM TMF 1800)--This was not used.

Band Pass Filter (PMI Model 1085A)--This is a virtually lossless filter with a bandpass from 8 to 10 GHz and was inserted between the output of the TWT and the crystal detector. Figure 12 displays the operating characteristics of this filter.

Silvered Mirror--A piece of a regular silvered coated mirror, approximately 4 inches by 6 inches, was used for optical alignment purposes.

Aluminum Plate--Five pieces of aluminum plate were used to cover outlet of beam tube. Each piece was situated flush with beam tube such that beam passed nearly normal through surface when in use. The pieces all measured 4 13/16 inches by 5 10/16 inches by 0.040 inches. One piece had no hole, one piece had a one inch hole drilled through it, another one had a 3/4 inch hole, another one had a 1/2 inch hole and the last piece had a 1/4 inch hole. The purpose of the hole was to study diffraction transition radiation. Two pieces of aluminum plate, measuring 10 inches by 14 inches by 0.040 inches, were used as reflecting mirrors. They differed only in the fact that one had a 3/8 inch hole drilled in it.

APPENDIX C

RECOMMENDATIONS FOR FUTURE WORK

1. Narrow scope of experiment and concentrate on investigation of diffraction transition radiation improving on accuracy and minimizing errors.

2. Investigate relationship between 11/16 inch exit beam window and production of transition and diffraction transition radiation.

3. In order to fill in missing data, complete this experiment using the solid reflecting mirror at the lower energies.

4. Investigate effect of hole in reflecting mirror.

5. Conduct this experiment at a larger interaction length, L, preferably at a National Laboratory such as Los Alamos, and investigate Cerenkov radiation at low energies or the effects of transition and diffraction transition radiation.

LIST OF REFERENCES

1. Jelley, J.V., Cerenkov Radiation and Its Applications, Pergamon Press, 1958.

2. Ter-Mikaelian, M.L., High-Energy Electromagnetic Processes In Condensed Media, Wiley-Interscience, 1972.

3. Buskirk, F.R. and Neighbours, J.R., "Cerenkov Radiation From Periodic Electron Bunches," Physical Review A, Volume 28, Number 3, September, 1983.

4. Buskirk, F.R. and Neighbours, J.R., Naval Postgraduate School, Report Number NPS-61-83-010, "Diffraction Effects in Cerenkov Radiation," June, 1983.

5. Bruce, R.G., Cerenkov Radiation From Periodic Bunches For A Finite Path In Air, Master's Thesis, Naval Postgraduate School, Monterey, California, 1985.

6. Skolnik, M.I., Introduction to Radar Systems, p. 229, McGraw-Hill, 1980.

7. Rule, D.W. and Fiorito, R.B., Naval Surface Weapons Center Technical Report Number NSWC TR 84-134, "The Use of Transition Radiation As A Diagnostic For Intense Beams," July 1984.

8. Ginsburg, V.L. and Frank, I.M., "Radiation of a Uniformly Moving Electron Due to its Transition from One Medium to Another," Zhurnal Eksperimental'noi i Teoreticheskoi Fiziki, Volume 16, p. 15, 1946.

9. Zrelov, V.P. and Ruzicka, J., "On the Role of Vavilov-Cherenkov Radiation in Experiments on Optical Transition Radiation,' Nuclear Instruments and Methods, Volume 165, p. 91, 1979.

10. Bass, F.G. and Yakovenko, V.M., "Theory of Radiation from a Charge Passing Through an Electrically Inhomogeneous Medium," Soviet Physics Uspeckhi, Volume 8, Number 3, p. 420, 1965.

11. Panofsky, W.K.H. and Phillips, M., Classical Electricity and Magnetism, pp. 341-353, Addison-Wesley, 1962.

12. Turner, E.R., Form Factor Effects on Microwave Cerenkov Radiation, Master's Thesis, Naval Postgraduate School, Monterey, California, 1984.

13. Vujaklija, M., Cerenkov Radiation from Periodic Electron Bunches for Finite Emission Length in Air, Master's Thesis, Naval Postgraduate School, Monterey, California, 1984.

INITIAL DISTRIBUTION LIST

		No. Copies
1.	Defense Technical Information Center Cameron Station Alexandria, Virginia 22304-6145	2
2.	Library, Code 0142 Naval Postgraduate School Monterey, California 93943-5000	2
3.	Physics Library, Code 61 Department of Physics Naval Postgraduate School Monterey, California 93943-5000	2
4.	Professor F.R. Buskirk, Code 61Bs Department of Physics Naval Postgraduate School Monterey, California 93943-5000	5
5.	Professor J.R. Neighbours, Code 61Nb Department of Physics Naval Postgraduate School Monterey, California 93943-5000	5
6.	Professor X.K. Maruyama B108, Bldg. 245 National Bureau of Standards Gaithersburg, Maryland 20899	2
7.	Dr. Donald Rule, Code R41 Naval Surface Weapons Center White Oak Laboratory 10901 New Hampshire Avenue Silver Springs, Maryland 20903-5000	2
8.	Dr. Ralph Fiorito, Code R41 Naval Surface Weapons Center White Oak Laboratory 10901 New Hampshire Avenue Silver Springs, Maryland 20903-5000	2
9.	Dr. Joseph Mack M4, M.S. P-940 Los Alamos National Laboratory Los Alamos, New Mexico 87545	2

10. LCDR Arthur J. O'Grady 2
Sub-Board of Inspection & Survey, Atlantic
Naval Amphibious Base
Norfolk, Virginia 23520-5300

11. Dr. James N. McMullin 1
18115-62B Avenue
Edmonton, Alberta Canada T5T 3J9

END

1-87

DTIC